

On the mean profiles of radio pulsars

V. S. Beskin^{1*} and A. A. Philippov^{1,2}

¹*P.N.Lebedev Physical Institute, Leninsky prosp., 53, Moscow, 119991, Russia*

²*Moscow Institute of Physics and Technology, Dolgoprudny, Moscow region, 141700, Russia*

4 May 2022

ABSTRACT

We study the influence of the propagation effects on the mean profiles of radio pulsars using the method of the wave propagation in the inhomogeneous media describing by Kravtsov & Orlov (1990). This approach allows us firstly to include into consideration the transition from geometrical optics to vacuum propagation, the cyclotron absorption, and the wave refraction simultaneously. In addition, non-dipole magnetic field configuration, drift motion of plasma particles, and their realistic energy distribution are taken into account. It is confirmed that for ordinary pulsars (period $P \sim 1$ s, surface magnetic field $B_0 \sim 10^{12}$ G) and typical plasma generation near magnetic poles (the multiplicity parameter $\lambda = n/n_{GJ} \sim 10^3$) the polarization is formed inside the light cylinder at the distance $r_{\text{esc}} \sim 1000R$ from the neutron star, the circular polarization being 5–20% which is just observed. The one-to-one correspondence between the signs of circular polarization and position angle (*p.a.*) derivative along the profile for both ordinary and extraordinary waves is predicted. Using numerical integration we now can model the main profiles of radio pulsars. It is shown that the standard *S*-shape form of the *p.a.* swing can be realized for small enough multiplicity λ and large enough bulk Lorentz factor γ only. It is also shown that the value of *p.a.* maximum derivative, that is often used for determination the angle between magnetic dipole and rotation axis, significantly depends on the plasma parameters [and differs from rotation vector model (RVM) value] and, hence, cannot be used without more precise specifying of magnetospheric plasma model.

Key words: Neutron stars— radio pulsars — polarization

1 INTRODUCTION

More than forty years after discovery, our understanding of pulsar phenomenon leaves a double impression. On the one hand, the key properties were understood almost immediately (see, e.g., the monographs by Manchester & Taylor, 1977, Lyne & Graham-Smith, 1998): the stable pattern of radio emission is related to the neutron star rotation, the energy source is the kinetic energy of its rotation, and the release mechanism has the electromagnetic nature. The mean profiles of radio pulsars are well described by the hollow cone model. Within four last decades enormous amount of observational data concerning polarization and other morphological properties of mean profiles was collected (Johnston et al., 2007, Weltevredre & Johnston (2008) Hankins & Rankin 2010, Keith et al., 2010, Yan et al., 2011). On the other hand, the common point of view on the mechanism of coherent radio emission is absent up to now (Beskin, 1999, Usov, 2006, Lyubarsky, 2008).

Any self-consistent theory of pulsar radio emission must include at least three main elements: first, the mechanism of the initial instability that leads to an inverse population in the maser mechanism of coherence or to the formation of charged bunches in the antenna mechanism; second, the saturation mechanism that determines the intensity of the outgoing radio emission; and, finally, the effects of radio wave propagation in the neutron star magnetosphere that determine the radiation beam. A quantitative comparison of the theoretical predictions for the generation of radio emission with observational data cannot be made without quantitative propagation theory.

As for initial instability, there are several proposed mechanisms: unstable flow of relativistic electron-positron plasma flowing along curved magnetic field lines (Goldreich & Keeley, 1971, Blandford, 1975, Asseo et al., 1980, Beskin, Gurevich & Istomin, 1993); instability caused by boundedness of the region of open field lines (Asseo, 1995, Luo, Melrose, Machabeli, 1994); the instability connected with kinetic effects, that can be caused by non-equilibrium of the particles energy distribution function (mainly, anomalous Doppler ef-

* E-mail: beskin@lpi.ru

fect in the region of cyclotron resonance); two-stream instability (Kazbegi, Machabeli, Melikidze, 1991); the instability connected with the nonstationarity of plasma particle production in the region of its generation (Lyubarskii, 1996). The saturation mechanism, whose investigation requires involving the effects of a nonlinear wave interaction, is the most complex from the theoretical point of view. Therefore, it is not surprising that only a few researchers have managed to consider this question consistently (see, e.g., Istomin, 1988). Finally, the processes of the wave propagation in pulsar magnetospheres have not yet been investigated with sufficient detail either, although the part of theory that includes the propagation processes can be constructed using the standard linear methods of plasma physics.

Recall that there are four assumptions in the hollow cone model: first, the emission is generated in the inner magnetospheric regions (where the magnetic field may be considered as a dipole); second, the emission propagates along the straight line; third, the cyclotron absorption may be neglected; and fourth, the polarization is determined at the emission point. Such basic characteristics of the received radio emission allows to determine the change of the position angle *p.a.* of the linear polarization along the mean profile (Manchester & Taylor, 1977)

$$p.a. = \arctan \left(\frac{\sin \chi \sin \phi}{\sin \chi \cos \zeta \cos \phi - \sin \zeta \cos \chi} \right). \quad (1)$$

Here χ is the inclination angle of the magnetic dipole to the rotation axis, ζ is the angle between the rotation axis and the observer's direction, and ϕ is the pulse phase.

As a result, the radiation beam width W_r and its statistical dependence on the period of pulsar P (Rankin, 1983, 1990), and also the existing of two orthogonal modes that naturally arise in a magnetoactive plasma, can be qualitatively explained under these assumptions. It is not surprising that the hollow cone model in its simplest realization is currently widely used for quantitative determination of the parameters of neutron stars (see, e.g., Taylor & Stinebring, 1986). At the same time, it is well known that, in general, three main assumptions are incorrect. First of all, after the paper by Barnard and Arons (1986), it became clear that the ordinary wave doesn't propagate in a straight line, but deflects away from the magnetic axis. Subsequently, this effect was studied in detail by Petrova and Lyubarskii (1998, 2000), it was an important element in the theory of Beskin et al. (1993). The correction to relation (1) connected with the aberration was determined by Blaskiewicz et al. (1991), but it was rare used in analysis of the observational data as well. Further, the cyclotron absorption that must take place near the light cylinder (Mikhailovsky et al. 1982) turns out to be so large that it will not allow the radio emission to escape the pulsar's magnetosphere (see, e.g., Fussell et al., 2003). Finally, the limiting polarization effect had not been discussed seriously over many years, although it was qualitatively clear that this effect must be decisive for explaining of high degree of circular polarization, typically 5–20%.

Indeed, in the region of the radio emission generation located at 10–100 neutron star radii, the magnetic field is still strong enough so the polarization of the two orthogonal modes is indistinguishable from a linear one. However, the assertions that the polarization characteristics are determined precisely in the emission region and the propagation

effects play no role can still be encountered in the literature (see, e.g., Mitra et al., 2009). Accordingly, in an overwhelming majority of the papers, Eqn. (1) is used to investigate the polarization.

Recall that the limiting polarization effect is related to the escape of radio emission from a region of dense plasma, where the propagation is well described in the geometrical optics approximation (in this case, the polarization ellipse is defined by the orientation of the external magnetic field in the picture plane), into the region of rarefied plasma, where the emission polarization becomes almost constant along the ray. This process was well studied (Zheleznyakov, 1977; Kravtsov & Orlov, 1990) and was used successfully for numerous objects, for example, in connection with the problems of solar radio emission (Zheleznyakov, 1964). However, in the theory of pulsar radio emission, such problem has not been solved. Above the papers where the level $r = r_{\text{esc}}$ at which the transition from the geometrical optics approximation to the vacuum occurs, was only estimated (see, e.g., Cheng & Ruderman 1979; Barnard, 1986), one can note only a few paper by Petrova and Lyubarskii (2000) (these authors considered the problem in the infinite magnetic field), by Petrova (2001, 2003, 2006), as well as the recent papers by Wang, Lai & Han (2010, 2011).

The goal of our paper is to consider all three main effects simultaneously in a consistent manner for realistic case. Not only the plasma density but also the magnetic field decrease with increasing distance from the neutron star will be included into consideration. Also, the non-dipole magnetic field, the drift motion of plasma particles, and realistic distribution function of outgoing plasma will be taken into account.

In section 2 both ordinary and extraordinary waves propagation in the pulsar magnetosphere is briefly considered. In section 3 the main parameters of our model including the hydrodynamic derivation of dielectric tensor of relativistic magnetized plasma as well as the magnetic field structure based on the force-free magnetosphere configuration obtained by Spitkovsky (2006), the particle energy and space distribution functions, and the cyclotron absorption are discussed. In section 4 the Kravtsov-Orlov equations allowing to include into consideration simultaneously the transition from geometrical optics to vacuum propagation, the cyclotron absorption, and the wave refraction are formulated. The results of numerical calculations of the mean profiles of radio pulsar are presented in section 5. Finally, in section 6 we discuss the main results of our consideration. In particular, it is shown that the standard *S*-shape form of the *p.a.* swing can be realized for small enough multiplicity λ and large enough bulk Lorentz factor γ only. It is also shown that the value of *p.a.* maximum derivative, that is often used for determination the angle between magnetic dipole and rotation axis, significantly depends from the plasma parameters [and differs from rotation vector model (RVM) value] and, hence, cannot be used without more precise specifying of magnetospheric plasma model.

2 TWO ORTHOGONAL MODES

2.1 On the number of outgoing waves

As was already stressed, the pulsar radio emission is highly polarized. The mean degree of linear polarization can reach 40–60%, and even 100% in some subpulses (Lyne & Graham-Smith, 1998). The analysis of the position angle demonstrates that in general pulsar radio emission consists of two orthogonal modes, i.e., two modes in which their position angles differ by 90° . It is logical to connect them with the ordinary (O-mode) and extraordinary (X-mode) waves propagating in magnetized plasma (Ginzburg, 1961).

Remember that starting from the pioneer paper by Barnard and Arons (1986), three waves propagating outward in the pulsar magnetosphere were commonly considered (see, e.g., Usov, 2006, Lyubarsky, 2008). The point is that in the most of papers (see, e.g., Melrose & Gedalin, 1999) the wave properties were considered in the comoving reference frame in which the plasma waves propagating outward and backward are identical. But in the laboratory reference frame (in which the plasma moves with the velocity $v \approx c$) the latter wave is to propagate outward as well. Thus, in reality we have four waves propagating outward.

As shown on Fig. 1, for $\theta = 0$ between the wave vector \mathbf{k} and external magnetic field \mathbf{B} two of them, n_1 and n_2 , correspond to transverse waves. For infinite external magnetic field $n_1 = n_2 = 1$. On the other hand, the waves n_3 and n_4 corresponds to plasma waves propagating in different directions in the comoving reference frame.

Moreover, as was demonstrated by Beskin, Gurevich & Istomin (1993), it is the fourth wave that is to be considered as the O-mode in the pulsar magnetosphere. Indeed, as shown in Fig. 1, for dense enough plasma in the radio generation domain for which $A_p \gg 1$ where

$$A_p = \frac{\omega_p^2}{\omega^2} < \gamma >, \quad (2)$$

it is this wave that propagates as transverse one at large angles θ , i.e., at large distances from the neutron star. Here $\omega_p = (4\pi e^2 n_e / m_e)^{1/2}$ is the plasma frequency, n_e is the particles number density, and $< \gamma >$ is the mean Lorentz-factor of the outflowing plasma. Two waves, for which the refractive index $n > 1$, cannot escape from the magnetosphere as at large distances they propagate along the magnetic field lines (and due to Landau damping, see Barnard & Arons, 1986).

In the hydrodynamical limit one can easily obtain the dispersion curves shown in Fig. 1 from the well-known dispersion equation for the infinite magnetic field (see, e.g., Petrova & Lyubarskii, 2000)

$$(1 - n^2 \cos^2 \theta) \left[1 - \frac{\omega_p^2}{\omega^2 \gamma^3 (1 - n v \cos \theta / c)^2} \right] - n^2 \sin^2 \theta = 0. \quad (3)$$

For $\theta \ll \theta^*$ and for $\theta \gg \theta^*$, where

$$\theta_* = < \frac{\omega_p^2}{\omega^2 \gamma^3} >^{1/4}, \quad (4)$$

there are two transverse and two plasma waves, but for $A_p \gg 1$ the nontrivial transformation from longitudinal to transverse wave takes place. It means that for $A_p \gg 1$ the mode n_4 can be emitted as a plasma wave, but it will escape from the magnetosphere as a transverse one.

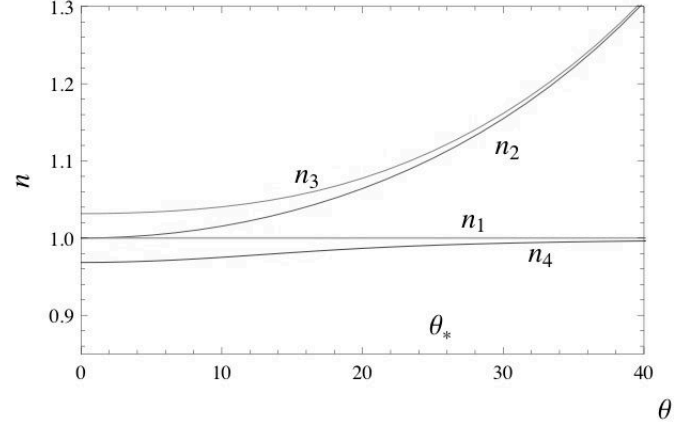


Figure 1. Dependence of the refractive indexes n on the angle θ between the wave vector \mathbf{k} and external magnetic field \mathbf{B} for $A_p \gg 1$. The lower branch corresponds to the O-mode

As the refractive index n_4 differs from unity, the appropriate ordinary mode is to deflect from the magnetic axis until $\theta \leq \theta^*$. As was already mentioned, for the O-mode this effect takes place until $A_p > 1$, i.e., for small enough distances from the neutron star $r < r_A$, where

$$r_A \approx 10^2 R \lambda_4^{1/3} \gamma_{100}^{1/3} B_{12}^{1/3} \nu_{\text{GHz}}^{-2/3} P^{-1/3}. \quad (5)$$

Here R , P , and B_{12} are the neutron star radius, rotation period (in s), and magnetic field (in 10^{12} G), respectively. Accordingly, $\gamma_{100} = \gamma/100$, ν_{GHz} is the wave frequency in GHz, and $\lambda_4 = \lambda/10^4$, where $\lambda = n_e/n_{\text{GJ}}$ is the multiplicity of the particle creation near magnetic poles ($n_{\text{GJ}} = \Omega B/2\pi c e$ is the Goldreich-Julian number density). On the other hand, the transverse extraordinary wave with the refractive index $n = 1$ (X-mode) is to propagate freely. As the radius r_A is much smaller than the escape radius r_{esc} (Cheng & Ruderman, 1979, Andrianov & Beskin, 2010)

$$r_{\text{esc}} \approx 10^3 R \lambda_4^{2/5} \gamma_{100}^{-6/5} B_{12}^{2/5} \nu_{\text{GHz}}^{-2/5} P^{-1/5}, \quad (6)$$

one can consider the effects of refraction and limiting polarization separately. In particular, this implies that one can consider the propagation of waves in the region $r \sim r_{\text{esc}}$ as rectilinear.

2.2 Extraordinary wave

Below for simplicity we assume that both two outgoing modes are generated at the same heights r_{em} (few to tens NS radii), where the magnetic field can be considered as a rotating dipole

$$\mathbf{B}(\phi) = -\frac{\mathbf{m}(\phi)}{r^3} + \frac{3\mathbf{r}}{r^5} (\mathbf{m}(\phi), \mathbf{r}). \quad (7)$$

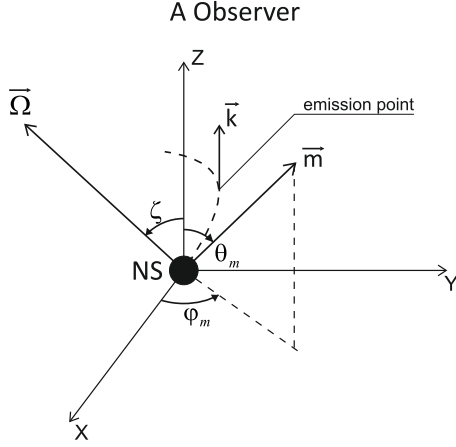
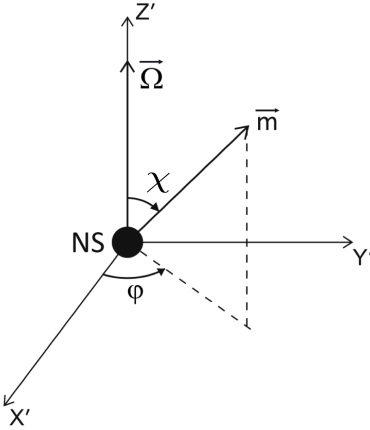
Here $\phi = \Omega t$ is the corresponding pulsar rotation phase.

In a fixed $X'Y'Z'$ frame (see Fig. 2) with the Z' -axis along the pulsar spin vector, and the line of sight in the $X'Z'$ -plane, we have

$$\mathbf{m}(\phi) = \sin \chi \cos \phi \mathbf{e}_{\mathbf{x}'} + \sin \chi \sin \phi \mathbf{e}_{\mathbf{y}'} + \cos \chi \mathbf{e}_{\mathbf{z}'}. \quad (8)$$

In the XYZ frame with the Z -axis along the line of sight we have

$$\mathbf{m}(\phi) = (\sin \chi \cos \phi \cos \zeta - \sin \zeta \cos \chi) \mathbf{e}_{\mathbf{x}} + \sin \chi \sin \phi \mathbf{e}_{\mathbf{y}}$$

Figure 2. *XYZ* frameFigure 3. *X'Y'Z'* frame

$$+(\cos\chi\cos\zeta + \sin\zeta\cos\phi\sin\chi)\mathbf{e}_z. \quad (9)$$

Therefore, in the *XYZ* reference frame (see Fig. 3) the spherical angles of the vector \mathbf{m} are

$$\cos\theta_m = \cos\chi\cos\zeta + \sin\chi\sin\zeta\cos\phi, \quad (10)$$

$$\tan\phi_m = -\frac{\sin\chi\sin\phi}{\sin\zeta\cos\chi - \sin\chi\cos\zeta\cos\phi}. \quad (11)$$

In the rotating vector model (RVM) the *p.a.* is determined purely by the projection of magnetic field on the sky's plane, so it coincides with ϕ_m . The sign of the arctan term is determined by the *p.a.* measured *counter-clockwise* in the picture plane, as it is common in radio astronomy (Everett & Weisberg, 2001). As the aberration angle in the initial point is approximately $\Omega r_{\text{em}}/c$, i.e., it is much smaller than the angular size of the emission cone $1/\gamma$, we can easily find the position of the emission point, where the tangential magnetic field line directs along the line of sight. This point $\mathbf{r}_{\text{em}} = (r_{\text{em}}, \theta_{\text{em}}, \phi_{\text{em}})$ in the *XYZ* frame is given by the spherical angles as

$$\theta_{\text{em}} = \frac{\theta_\mu}{2} - \frac{1}{2} \arcsin\left(\frac{1}{3} \sin\theta_m\right), \quad (12)$$

$$\phi_{\text{em}} = \phi_m. \quad (13)$$

Note that the impact angle ξ is the smallest angle between line of sight and magnetic moment \mathbf{m} , is given by $\xi = \chi - \zeta$. So the ray trajectory in the *XYZ* frame is given by the simple relation

$$\mathbf{R} = \mathbf{r}_{\text{em}} + r\mathbf{e}_z. \quad (14)$$

This relation allows us to determine magnetic field and all plasma characteristics along the ray.

2.3 Ordinary wave

Let us briefly review the main points of the theory of ordinary wave propagation (Barnard & Arons, 1986; Beskin et al., 1988; Petrova & Lyubarsky, 1990b). In the geometrical optics limit, the equations of motion of a ray are

$$\frac{d\rho_\perp}{dl} = \frac{\partial}{\partial k_\perp} \frac{k}{n_j}, \quad (15)$$

$$\frac{dk_\perp}{dl} = -\frac{\partial}{\partial \rho_\perp} \frac{k}{n_j}, \quad (16)$$

where ρ_\perp is the distance from the magnetic dipole axis, l is the coordinate along the ray, the index \perp corresponds to the components perpendicular to the dipole axis, e.g., $\theta_\perp = k_\perp/k$, and n_j are the corresponding refraction indexes. Below for simplicity the plasma density is assumed to be independent on the transverse coordinate ρ_\perp .

As the refraction of the O-mode takes place at small distances from the neutron star $r \ll r_A$ (5), the expressions for refraction indexes can be borrowed from the theory in the infinite magnetic field when the dielectric tensor of plasma has a form:

$$\varepsilon_{ij} = \begin{pmatrix} 1 & 0 & 0 \\ 0 & 1 & 0 \\ 0 & 0 & 1 - \langle \omega_p^2 / (\tilde{\omega}^2 \gamma^3) \rangle \end{pmatrix}. \quad (17)$$

Here and below by definition

$$\tilde{\omega} = \omega - (\mathbf{k}, \mathbf{v}), \quad (18)$$

and the brackets $\langle \rangle$ denote both the averaging over the particle distribution function $F_{e+,e-}(p)$ and the summation over the types of particles:

$$\langle \dots \rangle = \sum_{e+,e-} \int (\dots) F_{e+,e-}(p) d^3p. \quad (19)$$

As a result, for the ordinary mode the equations take the following form:

$$\frac{d\rho_\perp}{dl} = \frac{\theta_\perp + \alpha}{2}, \quad (20)$$

$$\frac{d\theta_\perp}{dl} = \frac{3}{4} \frac{\theta_\perp - \alpha}{l}, \quad (21)$$

where α is the inclination angle of the magnetic field line to the magnetic axis. As was shown in Beskin et al., (1993), for large enough angles $\theta \gg \theta^*$ (4) the ordinary wave propagates rectilinearly as well. From this condition and the solution of the equation above one can find

$$\theta_\perp(\infty) = \left(\frac{\Omega R}{c}\right)^{0.36} \left(\frac{1}{\omega^2} \left\langle \frac{\omega_{p0}^2}{\gamma^3} \right\rangle\right)^{0.07} f_{\text{em}}^{0.36} \left(\frac{l_r}{R}\right)^{0.15}. \quad (22)$$

Here ω_{p0} is the plasma frequency near the star surface, R is the neutron star radius, and index 'em' corresponds to the

quantities on the generation level. Besides, the dimensionless factor

$$f = \frac{c}{\Omega R} \left(\frac{l}{R} \right)^{-1} \sin^2 \theta_m \sim 1, \quad (23)$$

where the angle θ_m is measured from the magnetic axis, determines the position of the radiation point within the polar cap. The angle $W_r = 2\theta_\perp(\infty)$ is then determined the width of the directivity pattern. Finally, the "tearing off" level l_t defined by the condition $\theta = \theta^*$ is equals to

$$l_t = 2R \left(\frac{\Omega R}{c} \right)^{-0.48} \left(\frac{1}{\omega^2} \left\langle \frac{\omega_{p0}^2}{\gamma^3} \right\rangle \right)^{0.24} f_{\text{em}}^{-0.48} \left(\frac{l_{\text{em}}}{R} \right)^{-0.20}. \quad (24)$$

It gives

$$l_t \approx 40R P^{0.24} \nu_{\text{GHz}}^{-0.48} \gamma_{100}^{-0.72} B_{12}^{0.24} \lambda_4^{0.24} f_r^{-0.48} \left(\frac{l_{\text{em}}}{R} \right)^{-0.2}. \quad (25)$$

As we see, this level locates much deeper than the level of the formation of the outgoing polarization $r_{\text{esc}} \sim 1000 R$ (6). In more detail the procedure we have used is described in Appendix A.

3 MAGNETOSPHERE MODEL

3.1 Dielectric tensor

For reasonable parameters of the plasma filling the pulsar magnetosphere one can neglect the effect of curvature of magnetic field while considering the propagation of radio waves (see, e.g., Beskin, 1999). On the other hand, as the level of the formation of the outgoing polarization r_{esc} (6) locates in the vicinity of the light cylinder (Cheng & Ruderman 1979, Barnard, 1986), it is necessary to include into consideration the nonzero external electric field (Petrova & Lyubarskii, 2000). In this paragraph z -axis is selected along the direction of magnetic field and the wave vector lies in xz -plane.

Since that, our goal is to find the permittivity tensor of relativistic plasma in perpendicular uniform magnetic and electrical fields. In the derivation we take into account the

fact that the unpertubated motion of particles is the sum of the motion along the magnetic field lines and electrical drift:

$$\mathbf{V}_0 = V_\parallel \mathbf{b} + \mathbf{U}. \quad (26)$$

Here \mathbf{b} is the unit vector along the direction of magnetic field and $\mathbf{U} = c[\mathbf{E}, \mathbf{B}]/B^2$. In what follows we will use another form of this equation

$$\mathbf{V}_0 = [\mathbf{\Omega}, \mathbf{r}] + c i_\parallel \mathbf{B} \quad (27)$$

resulting from the condition $\mathbf{E} + [\mathbf{V}, \mathbf{B}]/c = 0$ (Beskin et al., 1993, Gruzinov, 2006).

To find the permittivity tensor ε_{ij} we have to find the motion of plasma particles in the homogeneous fields pertubated by the plane wave. We start from linearized Euler equation:

$$\left(\frac{\partial}{\partial t} + \mathbf{V}_0 \nabla \right) \delta \mathbf{P} = e \left(\delta \mathbf{E} + \left[\frac{\delta \mathbf{V}}{c}, \mathbf{B} \right] + \left[\frac{\mathbf{V}_0}{c}, \delta \mathbf{B} \right] \right), \quad (28)$$

$$\delta \mathbf{P} = m \gamma \delta \mathbf{V} + m \gamma^3 \frac{(\mathbf{V}_0, \delta \mathbf{V})}{c^2} \mathbf{V}_0, \quad (29)$$

and the relation between fields in the electromagnetic wave:

$$\delta \mathbf{B} = \frac{c}{\omega} [\mathbf{k}, \delta \mathbf{E}]. \quad (30)$$

Writing now the particle number density and electric current perturbations

$$\frac{\partial \delta n}{\partial t} + \text{div}(n \delta \mathbf{V} + \delta n \mathbf{V}_0) = 0, \quad (31)$$

$$\delta j_i = ne \delta V_i + \delta ne V_{0i} = \sigma_{ij} \delta E_j, \quad (32)$$

where σ_{ij} is a conductivity tensor, one can determine the permittivity tensor by the following relationship (Ginzburg, 1961)

$$\varepsilon_{ij} = \delta_{ij} + \frac{4\pi i}{\omega} \sigma_{ij}. \quad (33)$$

As a result, the expression for tensor in the infinite magnetic field looks like (the full expressions can be found in Appendix B):

$$\varepsilon_{ij} = \begin{pmatrix} 1 - \langle \frac{k_z^2 U_x^2 \omega_p^2 \gamma_U^2}{\tilde{\omega}^2 \gamma^3 \omega^2} \rangle & - \langle \frac{k_z^2 U_x U_y \omega_p^2 \gamma_U^2}{\tilde{\omega}^2 \gamma^3 \omega^2} \rangle & - \langle \frac{k_z U_x \omega_p^2 (\omega - k_x U_x) \gamma_U^2}{\tilde{\omega}^2 \gamma^3 \omega^2} \rangle \\ - \langle \frac{k_z^2 U_x U_y \omega_p^2 \gamma_U^2}{\tilde{\omega}^2 \gamma^3 \omega^2} \rangle & 1 - \langle \frac{k_z^2 U_y^2 \omega_p^2 \gamma_U^2}{\tilde{\omega}^2 \gamma^3 \omega^2} \rangle & - \langle \frac{k_z U_y \omega_p^2 (\omega - k_x U_x) \gamma_U^2}{\tilde{\omega}^2 \gamma^3 \omega^2} \rangle \\ - \langle \frac{k_z U_x \omega_p^2 (\omega - k_x U_x) \gamma_U^2}{\tilde{\omega}^2 \gamma^3 \omega^2} \rangle & - \langle \frac{k_z U_y \omega_p^2 (\omega - k_x U_x) \gamma_U^2}{\tilde{\omega}^2 \gamma^3 \omega^2} \rangle & 1 - \langle \frac{\omega_p^2 (\omega - k_x U_x)^2 \gamma_U^2}{\tilde{\omega}^2 \omega \gamma^3} \rangle \end{pmatrix} \quad (34)$$

Here now

$$\tilde{\omega} = \omega - k_x U_x - k_z v_\parallel, \quad (35)$$

and

$$\gamma_U = (1 - U^2/c^2)^{-1/2}. \quad (36)$$

3.2 Magnetic field structure

As the formation of the outgoing polariation locates in the vicinity of the light cylinder, it is necessary to include into consideration the corrections to the dipole magnetic

field which, actually, determines the disturbance of the S -shape form (1) of the $p.a.$ swing. In this work we discuss the following models of magnetic field

$$\mathbf{B} = \mathbf{B}_d + \mathbf{B}_w, \quad (37)$$

where the field \mathbf{B}_d connects with the dipole magnetic field of the neutron star, and the field \mathbf{B}_w corresponds to the outgoing wind.

For \mathbf{B}_d we discuss three possible models.

(i) The vacuum model, in which (for an orthogonal rotator) the magnetic field is described by the expressions (Lan-

dau & Lifshits, 1975)

$$B_r = \frac{|\mathbf{m}|}{r^3} \sin \theta \operatorname{Re} \left(2 - 2i \frac{\Omega r}{c} \right) E_x(r, \varphi, t), \quad (38)$$

$$B_\theta = \frac{|\mathbf{m}|}{r^3} \cos \theta \operatorname{Re} \left(-1 + i \frac{\Omega r}{c} + \frac{\Omega^2 r^2}{c^2} \right) E_x(r, \varphi, t), \quad (39)$$

$$B_\varphi = \frac{|\mathbf{m}|}{r^3} \operatorname{Re} \left(-i - \frac{\Omega r}{c} + i \frac{\Omega^2 r^2}{c^2} \right) E_x(r, \varphi, t), \quad (40)$$

where here and below

$$E_x(r, \varphi, t) = E_x(r, \varphi - \Omega t) = \exp \left(i \frac{\Omega r}{c} + i\varphi - i\Omega t \right). \quad (41)$$

(ii) The model of "non-rotating dipole", in which we neglect radiative corrections in the pre-exponential factors:

$$B_r = 2 \frac{|\mathbf{m}|}{r^3} \sin \theta \operatorname{Re} E_x(r, \varphi, t), \quad (42)$$

$$B_\theta = -\frac{|\mathbf{m}|}{r^3} \cos \theta \operatorname{Re} E_x(r, \varphi, t), \quad (43)$$

$$B_\varphi = -\frac{|\mathbf{m}|}{r^3} \operatorname{Re} i E_x(r, \varphi, t). \quad (44)$$

As a result, since the ray propagates almost along the radius, i.e. $r \approx ct$, the full compensation of time and radial contributions in the factor $\exp(i\Omega r/c + i\varphi - i\Omega t)$ takes place, so the ray does not feel the dipole rotation.

(iii) The model of filled magnetosphere, which corresponds to a rigidly rotating dipole,

$$B_r = 2 \frac{|\mathbf{m}|}{r^3} \sin \theta \operatorname{Re} \exp(i\varphi - i\Omega t), \quad (45)$$

$$B_\theta = -\frac{|\mathbf{m}|}{r^3} \cos \theta \operatorname{Re} \exp(i\varphi - i\Omega t), \quad (46)$$

$$B_\varphi = -\frac{|\mathbf{m}|}{r^3} \operatorname{Re} i \exp(i\varphi - i\Omega t). \quad (47)$$

Such a magnetic field at the distances $r < R_L$ was obtained by Beskin et al., (1993) and by Mestel et al., (1999) as a consistent solution of the force-free equation describing neutron star magnetosphere.

As to the wind component, we use the following expressions corresponding to the so-called "split monopole" solution (Michel, 1973; Bogovalov, 1999)

$$B_r = \frac{\Psi_{\text{tot}}}{2\pi r^2}, \quad (48)$$

$$B_\varphi = -f_\varphi \frac{\Psi_{\text{tot}}}{2\pi R_L} \frac{\sin \theta}{r}. \quad (49)$$

Here $\Psi_{\text{tot}} = 2\pi f_r (\Omega/c) |\mathbf{m}|$ is the total magnetic flux through the polar cap, and $f_r \sim 1$ and $f_\varphi \sim 1$ are the dimensionless constants. We see that the former term describe the quasi-monopole radial magnetic field. Such a structure was obtained not only for the axisymmetric force-free (Contopoulos et al., 1999, Timokhin, 2006) and MHD (Komissarov, 2006) numerical simulations but it describes good enough the magnetic field of the inclined rotator as well (Spitkovsky, 2006). As we are actually interesting in the disturbance of the dipole magnetic field inside the light cylinder only, we do not include here into consideration the switching of the radial field in the current sheet in the equatorial region. As the total magnetic flux through the polar cap depends only weakly on the inclination angle χ (Beskin et al., 1993, Spitkovsky, 2006), we put here for simplicity $f_r = 1$ (for zero longitudinal current f_r changes from 1.592 to 1.93).

Table 1. Models of the magnetic field structure

model	A	B	C	D
dipole	<i>ii</i>	<i>iii</i>	<i>ii</i>	<i>iii</i>
wind	$f_\varphi = 0$	$f_\varphi = 0$	$f_\varphi = 1$	$f_\varphi = 1$

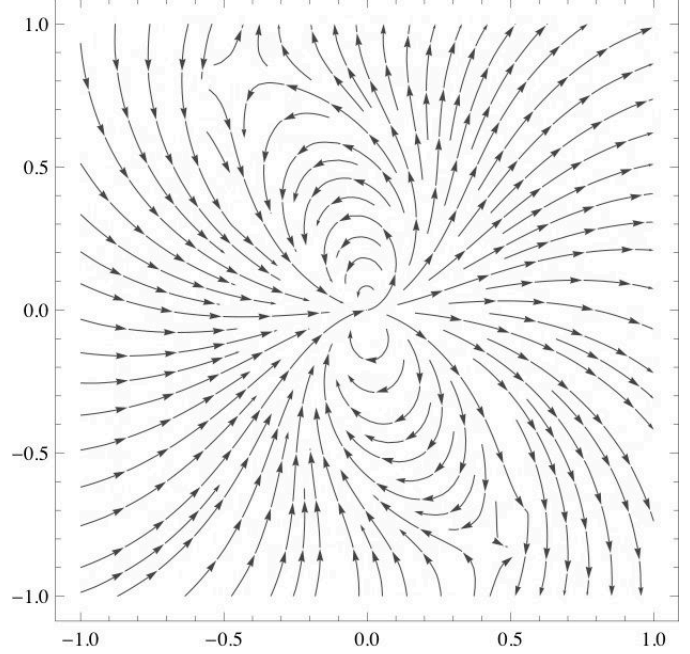


Figure 4. Structure of the magnetic field lines in equatorial plane in corotating frame for the orthogonal rotator $\chi = 90^\circ$. The magnetic field is considered as the sum of dipole and "split-monopole" (model D)

Besides, the latter term B_φ (49) corresponds to the toroidal magnetic field connected with the longitudinal electric current flowing in the magnetosphere. It is well-known that to support the MHD (in particular, force-free) outflow up to infinity the total longitudinal current I is to be close to the Michel (1973) current $I_M = \Omega \Psi_{\text{tot}} / 4\pi$ (Contopoulos et al., 1999). It corresponds to $f_\varphi \approx 1$. On the other hand, to realize this current for incline rotator with dipole magnetic field, it is necessary to suppose that the current density j_\parallel is to be much larger than the local Goldreich-Julian current $j_{\text{GJ}} \approx \Omega B \cos \chi / 2\pi$ (Beskin, 2010). As it is not clear whether the Michel current $I_M > I_{\text{GJ}}$ can be realized in the pulsar magnetosphere, in what follows the parameter f_φ can be considered as a free one.

In Table 1 we present the notation of the models which will be used in what follows. Magnetic field structure for model D (and for orthogonal rotator) is shown in Fig 4. Actually, it qualitatively coincides with the numerical model obtained by Spitkovsky (2006).

3.3 Plasma number density

Recall the well-known property of the one-photon particle production in a strong magnetic field: the secondary particles are produced only if the photon moves at large

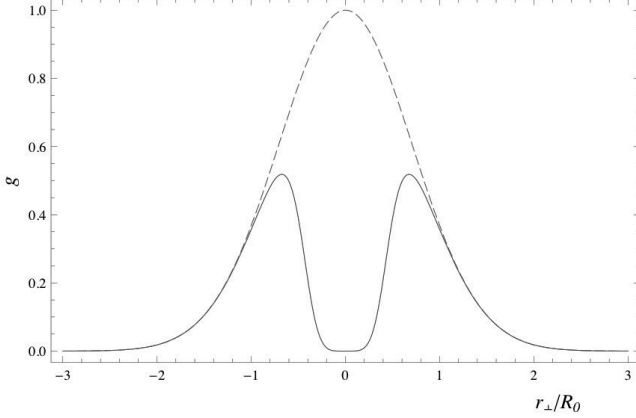


Figure 5. Plasma space distribution function $g(r_{\perp})$ on the polar cap as a function of the distance ρ from the magnetic axis for $f_0 = 0.25$. The dashed line corresponds to $f_0 = 0$

enough angle to the magnetic field line (Sturrock, 1971, Ruderman & Sutherland, 1975, Arons & Scharlemann, 1979). Since the relativistic particles near the neutron star surface can move only along the field line, so that the Lorentz factor $\gamma = (1 - v_{\parallel}^2/c^2)^{-1/2}$ (v_{\parallel} is the particle velocity along the magnetic field), the hard gamma-quanta emitted through curvature mechanism also begin to move along the field lines. As a result, the production of secondary particles will be suppressed near the magnetic poles, where the magnetic field is nearly rectilinear. Therefore, one would expect the secondary plasma density to decrease in the central region of the open field lines. It is this property that lies in the ground of the hollow cone model.

Bellow we assume that the plasma number density on a polar cap is known. It is convenient to write it down in the form

$$n_e(\theta_m, \varphi_m) = \lambda g(\theta_m, \varphi_m) n_{\text{GJ}}^{(0)}. \quad (50)$$

Here by definition $n_{\text{GJ}}^{(0)} = \Omega B / 2\pi c e$ is the amplitude of the Goldreich-Julian number density, i.e., it does not depend on the inclination angle χ . According to numerous calculations (Daugherty & Harding, 1982; Gurevich & Istomin, 1985; Medin & Lai, 2010) the multiplicity parameter

$$\lambda \sim 10^3 - 10^4. \quad (51)$$

Finally, the factor $g(\theta_m, \varphi_m) \sim 1$ depending on the magnetic pole angles θ_m and φ_m describes the real number density of the secondary plasma in the vicinity of the neutron star surface.

The procedure described below allows us to determine the properties of the outgoing radiation for arbitrary number density n within the polar cap. But in this work for simplicity we consider only the axially symmetric distribution

$$g(f) = \frac{\exp(-f^2) f^{2.5}}{f^{2.5} + f_0^{2.5}}, \quad (52)$$

where again $f = \rho_{\perp}^2 / R_0^2$ is the dimensionless distance to the magnetic axis ($R_0 = (\Omega R / c)^{1/2} R$ is the polar cap radius), and the parameter f_0 describes the hole size in space plasma distribution (see Fig. 5). It is natural to assume the intensity of radio emission in the emission region to be proportional

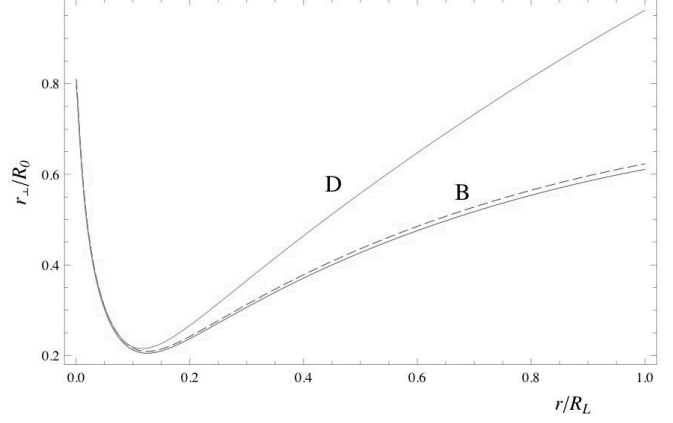


Figure 6. Dependences of the distance of the foot points to the magnetic axis within the polar cap as a function of the distance from the neutron star r for rotating dipole (model B) and for magnetic field including the monopole wind (model D) for the phase point $\phi = -5^\circ$. Dashed curve corresponds to analytical expression (60)

to the same function, as it is connected with the density of outgoing plasma.

To determine the number density n of the outgoing plasma in the arbitrary point of the magnetosphere, we use quasi-stationary formalism, which is valid for quantities that are functions of $\phi - \Omega t$. For such functions all the derivatives over time can be reduced to the derivatives over coordinates by the following rules (Beskin, 2009):

$$\frac{\partial}{\partial t} Q = -\Omega \frac{\partial}{\partial \phi} Q, \quad (53)$$

$$\frac{1}{c} \frac{\partial}{\partial t} \mathbf{V} = \text{rot}[\beta_{\mathbf{R}}, \mathbf{V}] - (\nabla \mathbf{V}) \beta_{\mathbf{R}}, \quad (54)$$

for any scalar (Q) and vector (\mathbf{V}) functions. Here by the definition

$$\beta_{\mathbf{R}} = \frac{[\Omega, \mathbf{r}]}{c}. \quad (55)$$

Using now the continuity equation

$$\frac{\partial n}{\partial t} + \text{div}(n \mathbf{V}_0) = 0, \quad (56)$$

where the velocity \mathbf{V}_0 is given by Eqn. (27), one can obtain

$$(\mathbf{B} \nabla)(n i_{\parallel}) = 0. \quad (57)$$

Hence, the product

$$n i_{\parallel} = \text{const} \quad (58)$$

remains constant along the field lines (Beskin et al., 1993, Gruzinov, 2006). Taking now into account only the first order by $\Omega r / c$ and assuming that the velocity of the outflowing particles is close to the light velocity c , we finally obtain

$$i_{\parallel} = \frac{1}{B} [1 - (\mathbf{b}, \beta_{\mathbf{R}})]. \quad (59)$$

Thus, to determine the number density n in the arbitrary point along the ray trajectory it is enough to know the number density and magnetic field at the base of a given field line on the neutron star surface. But for this it is necessary to produce the back integration along the field line from

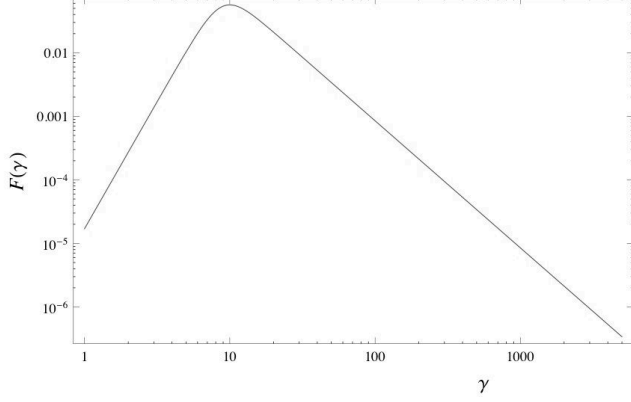


Figure 7. Particle energy distribution function

any point along the trajectory. In Fig. 6 we show the dependences of the distance of the foot points to the magnetic axis ρ_{\perp} within the polar cap as a function of the distance r from the neutron star for rotating dipole (model B) and for magnetic field including the monopole wind (model D) for the phase point $\phi = -5^{\circ}$. As for model A the appropriate value can be obtained analytically (dashed curve)

$$r_{\perp} = R \sqrt{\frac{R}{r}} \sin \vartheta_m, \quad (60)$$

where ϑ_m is the angle between local point on the ray vector and momentary magnetic axis, one can conclude that the precision of our procedure is high enough.

3.4 Energy distribution and cyclotron absorption

As was shown by Andrianov & Beskin (2010), for large enough shear of the magnetic field along the ray (as will be shown below, this condition does hold in the pulsar magnetosphere), all the polarization characteristics of outgoing radiation depend on the diagonal components of dielectric tensor, that are not sensitive to the difference of the e^+e^- distribution functions. This fundamental property allows us to consider the electron and positron energy distribution functions to be identical. Our particular choice is (see Fig. 7)

$$F(\gamma) = \frac{6\gamma_0}{2^{1/6}\pi} \frac{\gamma^4}{2\gamma^6 + \gamma_0^6}. \quad (61)$$

This distribution has the maximum for $\gamma = \gamma_0$ that is assumed as a typical Lorentz-factor of plasma particles, and has power-law spectrum γ^{-2} for large Lorentz-factors $\gamma \gg \gamma_0$. Thus, it models well enough the energy distribution function obtained numerically (Daugherty & Harding, 1982; Beskin et al., 1993).

Finally, consider the cyclotron absorption taking place in the region where the condition $\omega_B = \gamma\gamma_U\tilde{\omega}$ holds. As is well-known, the cyclotron resonance locates at the distances

$$r_{\text{res}} \approx 2 \cdot 10^3 R \nu_{\text{GHz}}^{-1/3} \gamma_{100}^{-1/3} B_{12}^{1/3} \theta_{0.1}^{-2/3} \quad (62)$$

comparable with the escape radius r_{esc} (6) (Mikhailovsky et al., 1982). It implies that these two effects are to be considered simultaneously. On the other hand, as was already stressed, in this region one can neglect the wave refraction, i.e., to put $\text{Re } n = 1$.

As a result, the intensity of outgoing radiation can be determined as

$$I_{\infty} = I_0 \exp(-\tau), \quad (63)$$

where I_0 is the intensity in the emission region, and the optical depth $\tau = 2\omega/c \int \text{Im } n \, dl$ can be found using the clear relation

$$\text{Im } n \approx \text{Im}(\varepsilon_{y'y'})/2. \quad (64)$$

As a result, we have

$$\begin{aligned} \tau &\approx \frac{4\pi^2 e^2}{m_e c} \int_0^{\infty} \int_0^{\infty} n_e(l) \frac{\tilde{\omega}}{\omega} F(\gamma) \delta\left(|\omega_B| \sqrt{1 - \frac{U^2}{c^2}} - \gamma \tilde{\omega}\right) d\gamma dl \\ &= \frac{4\pi^2 e^2}{mc} \int_0^{\infty} n(l) \frac{1}{\omega} F\left(\frac{|\omega_B| \sqrt{1 - U^2/c^2}}{\tilde{\omega}}\right) dl. \end{aligned} \quad (65)$$

Here we use the approximation $v_{\parallel}^2/c^2 \approx 1 - U^2/c^2$.

Remember that for evaluation one can use the simple relation (Mikhailovsky et al., 1982)

$$\tau \approx \lambda(1 - \cos\theta_{\text{res}}) \frac{r_{\text{res}}}{R_L}. \quad (66)$$

Hence, for $r_{\text{res}} \approx 0.1 R_L$, $\lambda \approx 10^4$, and $\theta_{\text{res}} \approx 0.1$ the optical depth is to be high enough ($\tau \approx 10$). On the other hand, as shown on Fig. 5 and Fig. 6, for $r_{\text{res}} \approx 0.1 R_L$ the ray passes the very central parts of the open field lines region where the plasma number density n can be much smaller than λn_{GJ} ($g(f) \ll 1$). For this reason, as will be shown below, the absorption of the outgoing radiation can be not so strong.

4 LIMITING POLARIZATION

The limiting polarization effect is well-known (Zheleznyakov, 1977). When the radiation escapes into a region of rarefied plasma, the wave polarization ceases to depend on the orientation of the external magnetic field. At the same time, in the domain of the dense enough plasma where the geometrical optics approximation is valid, the orientation of the polarization ellipse is to be determined by the direction of the external magnetic field. This implies that the geometrical optics approximation under weak anisotropy conditions becomes inapplicable and the question about the pattern of the limiting polarization effect should be solved by using the equations that describe a linear interaction of waves in an inhomogeneous magnetoactive plasma.

Traditionally to describe general radiative transfer in magnetoactive plasma four first-order differential equations (for all four Stokes parameters) are used (Sazonov, 1969, Zheleznyakov, 1996, Petrova & Lyubarskii, 1990, Broderick & Blandford, 2010, Wang et al., 2010, Scherbakov & Huang, 2011). Budden equation, i.e., the second-order equation to the complex function actually corresponds to the same approach (Budden, 1972, Zheleznyakov, 1977). On the other hand, both the standard and the Zheleznyakov-Budden approaches are not quite convenient for quantitative estimates of the polarization of the escaping emission in general case. But since we are going to describe the propagation of originally fully polarized waves, not the ansamble of waves, we actually

need only two equations for observable parameters, i.e., the position angle and the Stokes parameter V .

There exists a different approach that allows us immediately write down the equations for these observable quantities, namely, the Stokes parameter V , defining the circular polarization and the position angle $p.a.$, characterizing the orientation of polarization ellipse (Kravtsov & Orlov, 1990). This approach is valid in the quasi-isotropic case, i.e., in the case when the dielectric tensor can be presented as

$$\varepsilon_{ij} = \varepsilon \delta_{ij} + \chi_{ij}, \quad (67)$$

where the anisotropic part χ_{ij} is small as compared to isotropic one. In this case we have two small parameters — general WKB parameter $1/kL$ and

$$\Delta n/n_{1,2} \sim \chi_{ij}/n_{1,2} \ll 1. \quad (68)$$

In this case the solution can be found by expansion over this two small parameters.

As one can check, these conditions are just realized in the pulsar magnetosphere (Andrianov & Beskin, 2010). Indeed, in the region $r \sim r_{\text{esc}} \sim 10^3 R$ the value of $v = \omega_p^2/\omega^2$ $v \sim 10^{-7} \lambda_4 B_{12} \nu_{\text{GHz}}^{-2} P^{-1}$,

is much smaller than unity. Accordingly, the deviation of the refractive indices from unity, $|n_{1,2} - 1| \sim v$, is also very small here, so we can neglect the wave refraction in the polarization formation region.

The Kravtsov-Orlov equation

$$\frac{d\Theta}{dl} = \kappa + \frac{i\omega}{4c} [(\chi_{ba} - \chi_{ab}) + (\chi_{ba} + \chi_{ab}) \cos 2\Theta - (\chi_{aa} - \chi_{bb}) \sin 2\Theta], \quad (70)$$

is the equation for the complex angle $\Theta = \Theta_1 + i\Theta_2$, where Θ_1 is a position angle and Θ_2 determines the circular polarization by the relation

$$V = I \tanh 2\Theta_2. \quad (71)$$

Here I is the intensity of the wave. The components of the dielectric tensor χ_{ij} are to be written in a frame of unitary vectors \mathbf{a} and \mathbf{b} in the picture plane where \mathbf{a} is determined by the projection of the vector $\nabla \varepsilon$. Finally,

$$\kappa = 1/2(\mathbf{a} \cdot \nabla \times \mathbf{a} + \mathbf{b} \cdot \nabla \times \mathbf{b}) \quad (72)$$

is a ray torsion (see Kravtsov & Orlov, 1990 for more detail).

It can be easily understood that the rotation of position angle described by the ray torsion is fictitious and describes only the rotation of coordinate system. As a result, we can write down

$$\frac{d\Theta_1}{dl} = \frac{\omega}{2c} \text{Im}[\varepsilon_{x'y'}] - \frac{1}{2} \frac{\omega}{c} \Lambda \cos[2\Theta_1 - 2\beta(l) - 2\delta(l)] \sinh 2\Theta_2, \quad (73)$$

$$\frac{d\Theta_2}{dl} = \frac{1}{2} \frac{\omega}{c} \Lambda \sin[2\Theta_1 - 2\beta(l) - 2\delta(l)] \cosh 2\Theta_2. \quad (74)$$

Here l is a coordinate along the ray propagation, and the angle $\beta(l)$ defines the orientation of the external magnetic field in the picture plane. Further,

$$\Lambda = \mp \sqrt{(\text{Re}[\varepsilon_{x'y'}])^2 + \left(\frac{\varepsilon_{x'x'} - \varepsilon_{y'y'}}{2}\right)^2}, \quad (75)$$

where the signs correspond to the regions before/after the cyclotron resonance and

$$\tan(2\delta) = -\frac{2\text{Re}[\varepsilon_{x'y'}]}{\varepsilon_{y'y'} - \varepsilon_{x'x'}}. \quad (76)$$

We would like to note that in these equations the circular polarization is defined as it is common in radio astronomy (positive V corresponds to the co-clockwise rotating electric field vector for the observer). Finally, $\varepsilon_{i'j'}$ are the components of plasma dielectric tensor in the frame where the z -axis directs along the wave propagation and the external magnetic field lies in the xz -plane (see Appendix C). Non-relativistic version of the above equations is given in Czyz et al. (2007).

As we see, in the geometrical optics region Eqns. (73)–(74) describe the small oscillations of the angle Θ_1 near the value $\Theta_1 = \beta + \delta$. As the ray moves into the region of rarified plasma, the length of the spacial oscillations $L \sim c/(\omega \Delta n)$ increases and in the region $r > r_{\text{esc}}$ becomes larger than the characteristic length r . As a result, the angles Θ_1 and Θ_2 become constant for $r \gg r_{\text{esc}}$. They are the values that characterize the outgoing radiation.

As a result, the basic equations (73)–(74) generalize ones obtained by Andrianov & Beskin (2010) for zero drift velocity \mathbf{U} when $\text{Re}[\varepsilon_{x'y'}] = 0$ and, hence, $\delta = 0$. In particular, they now include into consideration the aberration effect considered by Blaskiewicz et al., (1991). This effect was also considered by Petrova & Lyubarskii (2000), but for the infinite magnetic field only. It is important that in Eqns. (73)–(74) the angle Θ_1 is measured relative to the laboratory frame because these equations contain the difference between Θ_1 and β only.

The equations above have the following important property. For homogeneous media ($\beta = \text{const}$, $\varepsilon_{ij} = \text{const}$) the parameters of polarization ellipse Θ_1 and Θ_2 remain constant if the following conditions are valid:

$$\Theta_1 = \beta + \delta, \quad \sinh 2\Theta_2 = \frac{\text{Im}[\varepsilon_{x'y'}]}{\Lambda} = -\frac{1}{Q}, \quad (77)$$

$$\Theta_1 = \beta + \delta + \pi/2, \quad \sinh 2\Theta_2 = -\frac{\text{Im}[\varepsilon_{x'y'}]}{\Lambda} = \frac{1}{Q}. \quad (78)$$

Here (see Appendix D for more detail)

$$Q = i \frac{\varepsilon_{y'y'} - \varepsilon_{x'x'}}{2\varepsilon_{x'y'}}. \quad (79)$$

This closely corresponds to the polarization of the two normal modes, the former corresponding to the O-mode, and the latter to the X-mode. In addition, the following important property holds: irrespective of the pattern of change in plasma density and magnetic field along the trajectory, if two modes were orthogonally polarized in the beginning ($\Theta_1^{(1)} - \Theta_1^{(2)} = \pi/2$, $\Theta_2^{(1)} = -\Theta_2^{(2)}$), then this property will also be retained subsequently, including the region where the geometrical optics approximation breaks down.

Finally it is easy to check that for high enough shear of the external magnetic field along the ray propagation (when the derivative $d(\beta + \delta)/dx$ is high enough), the first term in the r.h.s. of Eqn. (73) may be neglected. Hence, in this region $d\Theta_1/dl \approx d(\beta + \delta)/dl$. As a result, in this case the circular polarization in the region where the geometrical optics is valid will be defined by the diagonal (i.e., weakly dependent on the particle distribution function) dielectric tensor components χ_{aa} and χ_{bb} . This fundamental property is well-known in plasma physics and crystal optics (see, e.g.,

Zheleznyakov et al., 1983, Czyz et al., 2007), but up to now it was not used in connection with the pulsar radio emission.

As a result, one can write down

$$\frac{V}{I} \approx \frac{1}{|Q|} \frac{d(\beta + \delta)/dx}{A} \frac{1}{\cos[2\Theta_1 - 2\beta(l) - 2\delta(l)]}. \quad (80)$$

Here

$$A = |v_{\parallel}/c(1 - \sin\theta U_x/c) - \cos\theta(1 - U^2/c^2)|, \quad (81)$$

$x = \Omega/c$, and we used Goldreich-Julian expression for the plasma density. Consequently, the sign of the circular polarization will coincide with the sign of the derivative $d(\beta + \delta)/dx$ for the O-mode and they must be opposite for the X-mode. Remember, that this approximation is valid for large enough derivative $d(\beta + \delta)/dx \sim 1$ (i.e., for large enough total turn $\Delta(\beta + \delta) \sim 1$ within the light cylinder $R_L = c/\Omega$), and for small angle of propagation $\theta \ll 1$ through the relativistic plasma ($v_{\parallel}/c \sim 1$). Both these conditions in the magnetospheres of radio pulsars are valid with a good accuracy. Under these conditions and assuming that $U/c \ll 1$ and $U_x/c \approx U/c \approx \theta$ one can obtain

$$A \approx \frac{\theta^2}{2} - \frac{1}{2\gamma^2} - \frac{U_x}{c} \sin\theta + \frac{U^2}{c^2} \approx \frac{\theta^2}{2} - \frac{1}{2\gamma^2} \ll 1. \quad (82)$$

So, the Stokes parameter V (81) is indeed much larger than $V_0/I = \pm 1/Q$ resulting from standard evaluation (Ginzburg, 1961).

Finally, our numerical simulations show that the sign of the derivative $d(\beta + \delta)/dx$ is opposite to the sign of $dp.a./d\phi$. As one can see from Eqn. (80), this results in an important prediction:

- For the X-mode the signs of the circular polarization V and the derivative $dp.a./d\phi$ should be the SAME.
- For the O-mode the signs of the circular polarization V and the derivative $dp.a./d\phi$ should be OPPOSITE.

This implies also that the effects of the particle drift motion, as was already found by Blaskiewicz et al. (1991) (see also Hibschan & Arons, 2001), shifts the $p.a.$ curve to the trailing part of the mean profile.

5 RESULTS

Thus, in addition to effects considered by Andrianov & Beskin (2010), in this paper the arbitrary non-dipole magnetic field configuration, arbitrary number density profile within the polar cap, the drift motion of plasma particles, and their realistic energy distribution function are taken into account. It gives us the first opportunity to provide the quantitative comparison of the theoretical predictions with observational data. Using numerical integration we can now model the mean profiles of radio pulsars and, hence, evaluate the physical parameters of the plasma flowing in the pulsar magnetosphere.

As was already demonstrated by Beskin & Philippov (2011), the morphological properties of the mean profiles of radio pulsars are in good agreement with the theory predictions. E.g., as shown in Table 2, for more than 70 pulsars collected from two reviews by Weltevrede & Johnston (2008) and Hankins & Rankin (2010), most pulsars with double (D)

Table 2. Statistics of pulsars with known circular polarization V and position angle swing. Pulsar period P is in seconds, and the window width W_{50} is in degrees.

Profile	O _S	O _D	X _S	X _D
Number	6	23	45	6
$\sqrt{P}W_{50}$	6.8 ± 3.1	10.7 ± 4.5	6.5 ± 2.9	5.3 ± 3.0

mean profile corresponds to the O-mode (they have the opposite signs of V and $dp.a./d\phi$), and the most pulsars with single (S) mean profiles corresponds to the X-mode (they have the same signs of V and $dp.a./d\phi$). Moreover, statistically the O-mode pulsars have wider mean pulses than X-mode ones.

Detailed discussion of the morphological properties of mean profiles is beyond the scope of our consideration. The goal of this paper is in quantitative analysis of the propagation effects on the polarization characteristics of radio pulsars. In particular, we try to determine how the plasma parameters affect the S -shape of the position angle swing and the properties of the mean profile.

5.1 Ordinary pulsars

At first, let us discuss the results obtained by numerical integration of equations (73)–(74) for "ordinary" pulsar (its parameters are given in Table 3). Everywhere below the dashed curves on the intensity panel show the intensity profile without any absorption (we suppose that it repeats the particle number density profile shown in Fig. 5). If the dashed curve is not shown, then the absorption is fatal and only the original intensity (which is normalized to 100 in its maximum) is shown. The dashed curves on $p.a.$ panels show the prediction of the RVM-model (1).

On Fig. 8 we show the $p.a.$ swing and the intensity I_{∞} (63) for extraordinary O-mode as a function of the pulsar phase ϕ for "non-rotating dipole" without the wind component (model A); the drift effects are neglected as well. The circular polarization degree does not exceed one percent here and that is why this curve is not presented in this picture. It results from approximately constant β in this case. For this reason, as we see, the $p.a.$ curve is nicely fitting by the RVM model.

Further, the upper solid line corresponds to $f_0 = 0.25$, and the lower one corresponds to $f_0 = 0.0025$. The lower intensity curve shows that for $f_0 = 0.0025$ ($r_{\perp}/R_0 = 0.05$) the absorption is fatal and the emission can not escape from the magnetosphere. As was already stressed, this property can be easily explained. Indeed, for $f_0 \ll 1$ the rarified region of the "hollow cone" is actually absent, and the rays pass the cyclotron resonance in the region of rather dense plasma. On the other hand, for $f_0 \approx 1$ the number density in the region of the cyclotron resonance is low enough for rays to escape the magnetosphere without strong absorption.

On Fig. 9 we show the $p.a.$ swing (low panels), the intensity I_{∞} (solid lines on the top panels), and the Stokes parameter V (dotted lines) as a function of the pulsar phase ϕ for extraordinary wave for magnetic field model C and for various multiplicity parameter λ . It is obvious that the absorption increases with increasing λ . In most cases, the

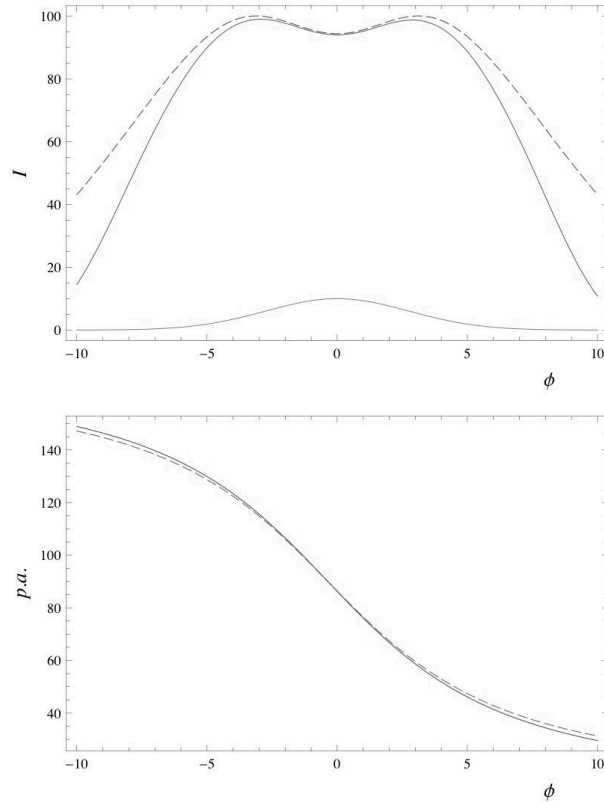


Figure 8. The $p.a.$ swing and the intensity I_∞ (63) as functions of the pulsar phase ϕ for "non-rotating dipole" (model A). Here and below the dashed curves on the intensity panel show the intensity profile without any absorption. The upper solid line corresponds to $f_0 = 0.25$, and the lower one – to $f_0 = 0.0025$

Table 3. Parameters of the 'ordinary' pulsar

P	B_0	χ	ζ	f_0	r_{rad}	γ	λ
1 s	10^{12} G	45°	48°	0.25	$30R$	50	10^3

trailing part of the mean profile is absorbed (see Dyks et al., 2010 as well).

Besides, as one can see, the $p.a.$ curves differ significantly from the RVM one (dashed lines) as λ growing. This property can be easily understood as well. Indeed, as the escape radius r_{esc} (6) increases as $\lambda^{2/5}$, for large enough λ the polarization properties of the outgoing waves are to be formed in the vicinity of the light cylinder, i.e., in the region with quasi-homogeneous magnetic field (see Fig. 4).

Further, as was already mentioned, the drift effect causes the $p.a.$ curve to be shifted to the trailing part of the mean profile. It is necessary to stress that the opposite shift is to take place if we neglect the drift effect on the dielectric tensor (Andrianov & Beskin, 2010, Wang et al., 2010). One can note that for high values of multiplicity parameter (i.e., for full absorption of the trailing part of the mean pulse) the observer will detect approximately constant $p.a.$ Finally, as one can see from Eqn. (81), the maximum of circular polarization is also shifted to the trailing side, as larger deviations from the S -shape produce larger circular polarization. It is not visible on this picture because

the trailing side of the beam is absorbed. Detailed analysis of observational confirmations of this effect needs a special investigation.

On Fig. 10 we show the same dependences for various Lorentz-factors of outgoing plasma $\gamma_0 = 10, 100$, and 300 . As the escape radius r_{esc} (6) decreases as $\gamma^{-6/5}$, the largest shift of the $p.a.$ curve takes place for small $\gamma_0 = 10$. Finally, on Fig. 11 one can see the same dependences for various wave frequencies $\nu = 0.03, 0.2$, and 0.5 GHz. As $r_{\text{esc}} \propto \nu^{-2/5}$, the largest shift of the $p.a.$ curve takes place for small frequencies. One can note that the full investigation of frequency dependence of main profiles of radio pulsars is more complicate and must include, e.g., the detailed analysis of frequency dependence of the emissin radius r_{rad} (Beskin et al., 1993). This is beyond the scope of the article.

As was demonstrated above, in general the sign of the circular polarization remains constant for a given mode. But under certain conditions the change of the V sign in the same mode may occur. It can take place when we cross the directivity pattern in the very vicinity of the magnetic axis. Such an example for the X-mode is shown on Fig. 12 for $P = 1\text{ s}$, $\zeta = 49^\circ$, $\chi = 48.5^\circ$, $\lambda = 10^3$, $\gamma = 50$, $R_0 = 100 R$.

Finally, in Table 4 we present the values of maximum derivative $(dp.a./d\phi)_{\text{max}}$, that is commonly used for determination of the inclination angle χ (see, e.g., Kuzmin & Dagkesamanskaya, 1983, Malov, 1990, Everett & Weisberg, 2001). As we see, these values significantly depend on the plasma parameters (and can differ drastically from the RVM

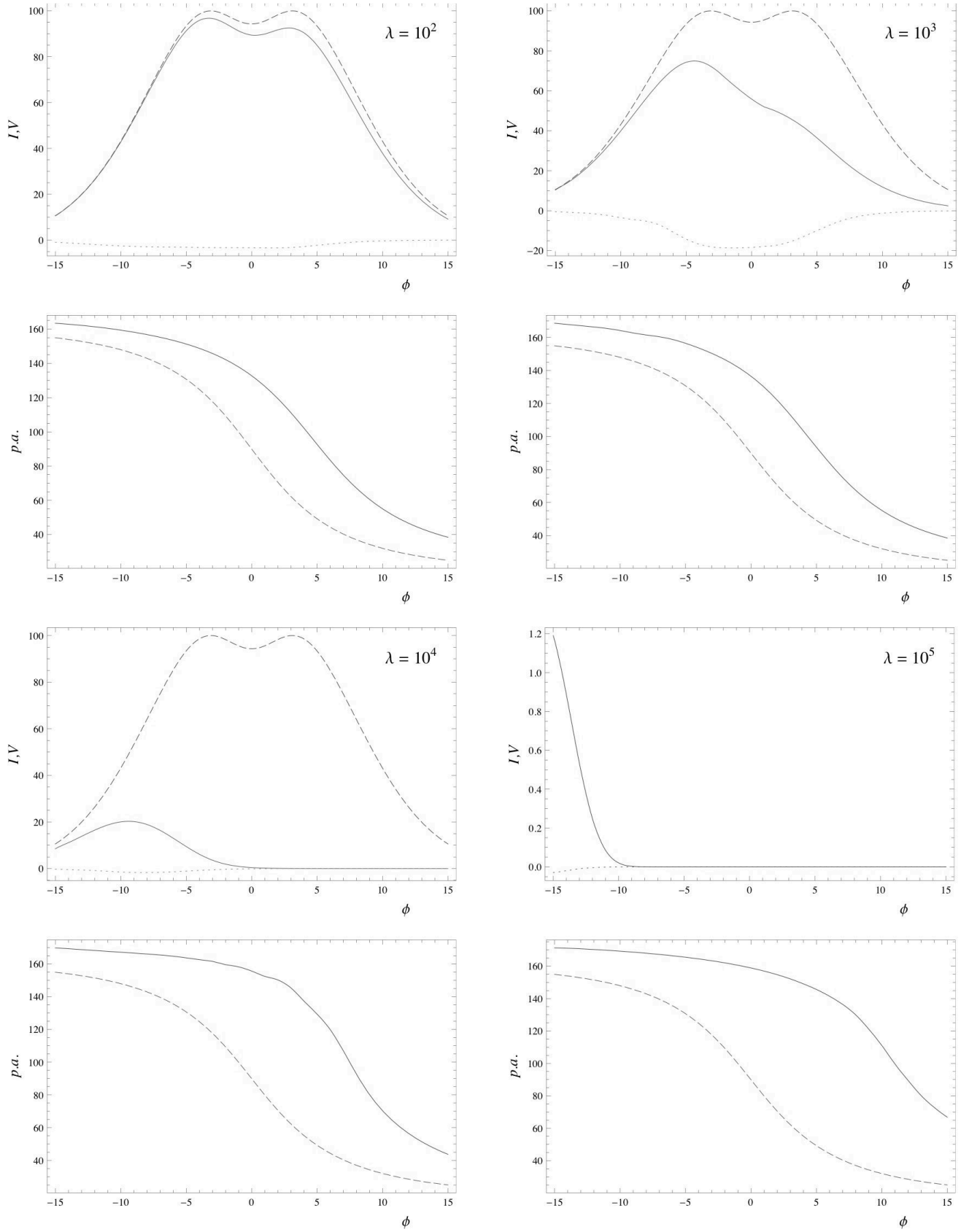


Figure 9. The same for model C and for different multiplicity factors $\lambda = 10^2, 10^3, 10^4$, and 10^5 . Here $\gamma = 50$ and $\nu = 1\text{GHz}$. Dotted line corresponds to Stokes parameter V

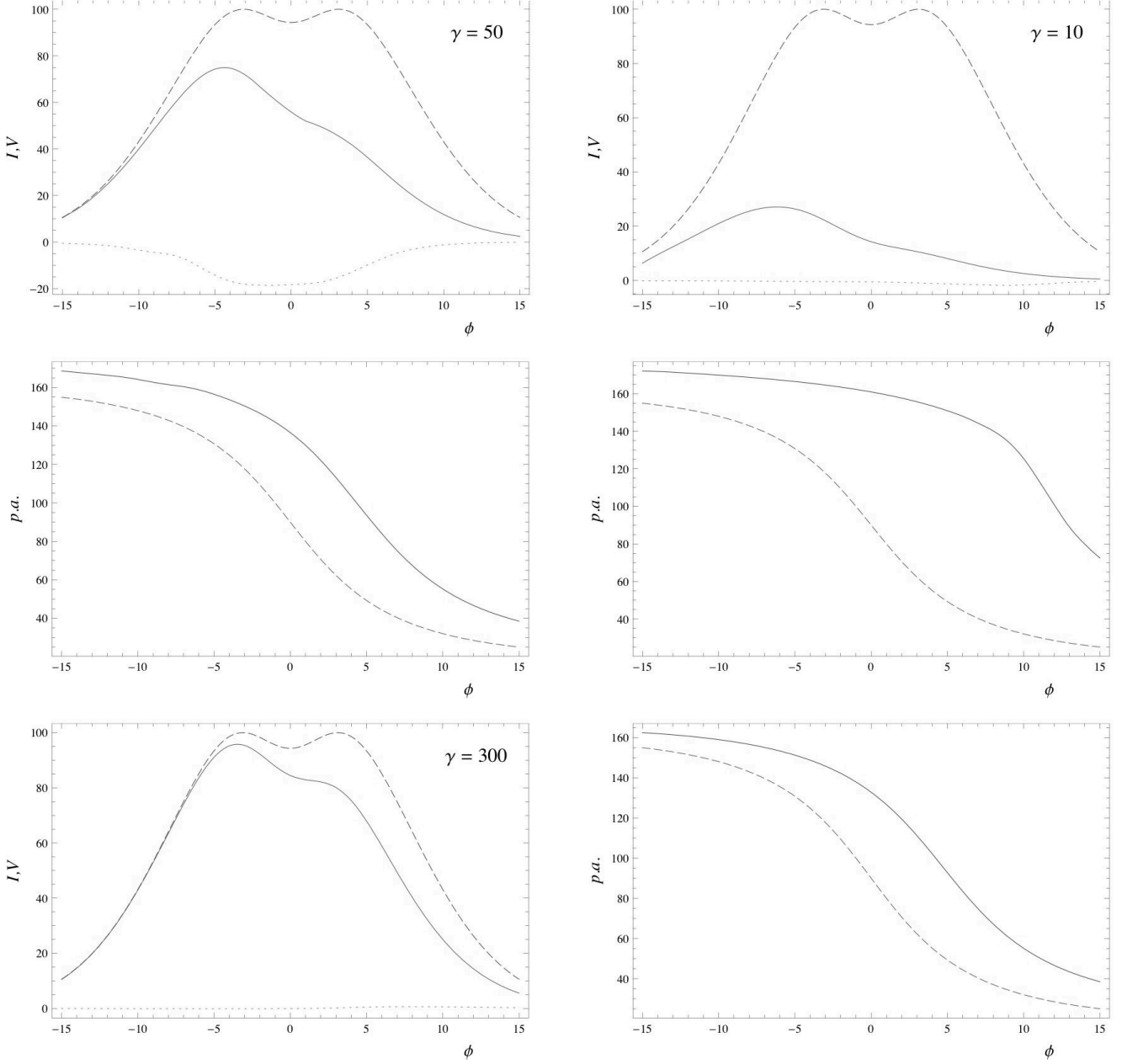


Figure 10. The same for various Lorentz-factors $\gamma_0 = 10, 100$, and 300 . Here $\lambda = 10^3$, and $\nu = 1\text{GHz}$

value). Hence, more precise specifying of magnetospheric and plasma model is necessary for quantitative analysis of the pulsar characteristics. In our opinion, this technique can be applied when the whole S -swing is detected. Otherwise the situation like in Fig. 9 for $\lambda = 10^4$ may occur. Also, if one try to fit the whole $p.a.$ curve by the RVM function (1) the unexpected result may take place. It is nicely fitted by the RVM model with non-zero shift value (13), but with the angles $\zeta = 97^\circ$ and $\chi = 93^\circ$ that drastically differ from real ones (see Fig. 13 and Table 3)!

5.2 Two modes profiles

On Fig. 14 an examples of the mean profiles including two orthogonal modes are presented. The ratio of the inten-

sities in the radiation domain $r = r_{\text{rad}}$ was assumed to be $I_O^{(0)}/I_X^{(0)} = 1/3$. The jumps in the $p.a.$ curves were done at the phase ϕ where $I_O = I_X$. As we see, this jump can differ from 90° . This results from the different trajectories of two orthogonal modes. It is necessary to stress that in our consideration the ratio $I_O^{(0)}/I_X^{(0)}$ is free, and its precise determination is a question for the radio emission generation theory.

We see that for radio pulsars for which two modes can be observed the mean profiles are indeed to have the triple form. As the O-mode deviates from magnetic axis, we have to see the O-mode in the leading part, the X-mode in the centre, and again the O-mode in the trailing part of the mean profile. As was demonstrated by Beskin & Philippov (2010), radio pulsars with triple mean profile in general have such

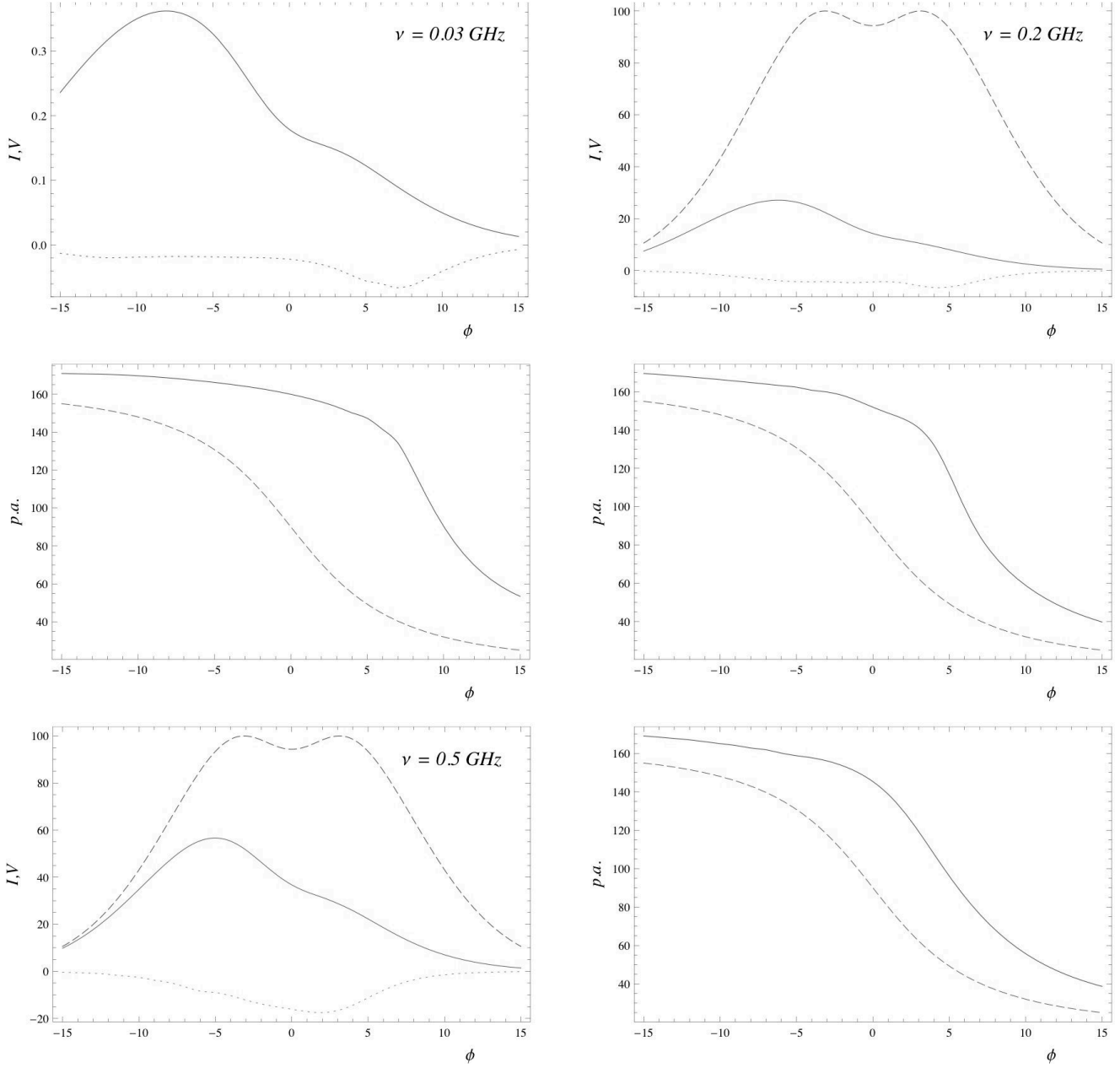


Figure 11. The same for model C and for various frequencies $\nu = 0.03, 0.2$, and 0.5 GHz. Here $\lambda = 10^3$, and $\gamma = 50$

a morphological structure. The detailed analysis is beyond the scope of our present consideration.

5.3 Millisecond pulsars

As the last example, on Fig. 15 we show the mean profiles obtained for millisecond pulsar (the parameters are given in Table 5). One important feature appearing here is that the leading, not trailing part of the mean profile can be absorbed. It is caused by the bending of the open field lines tube near the light cylinder due to non-dipolar magnetic field. As a result, the cyclotron resonance takes place in the region of rarefied plasma for the trailing part of the pulse. Also, stronger deviations from the S -shape of $p.a.$ swing are

Table 5. Parameters of the millisecond pulsar

P	B_0	χ	ζ	f_0	r_{rad}	γ	λ
20 ms	10^8 G	45°	48°	0.04	$1.25R$	50	10^3

found as compared to the case of ordinary pulsar, because polarization forms closer to the light cylinder.

6 DISCUSSION AND CONCLUSIONS

In this paper we study the influence of the propagation effects on the mean profiles of radio pulsars. The Kravtsov-Orlov approach allows us firstly to include into considera-

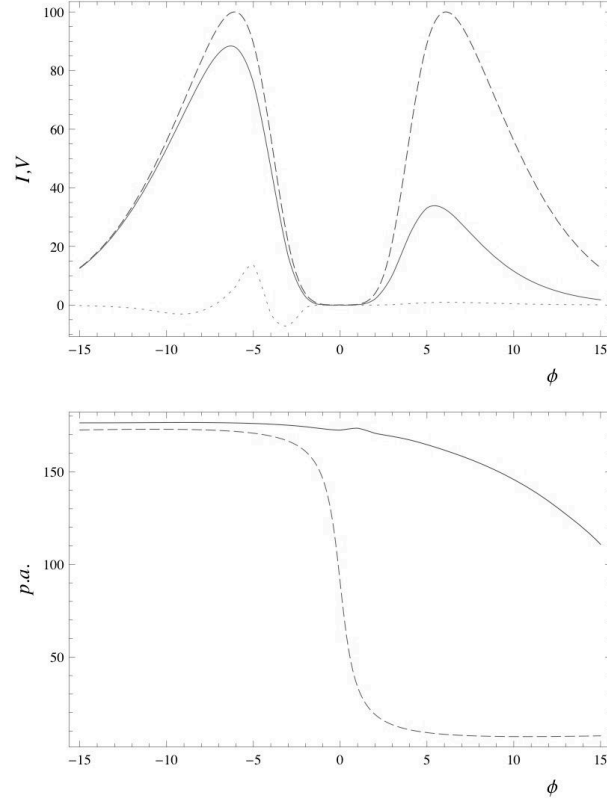


Figure 12. The results of simulations for X-mode, $P = 1s$, $\zeta = 49^\circ$, $\chi = 48.5^\circ$, $\lambda = 10^3$, $\gamma = 50$, $R_0 = 100R$. It shows that under certain conditions change of V sign in the same mode may occur

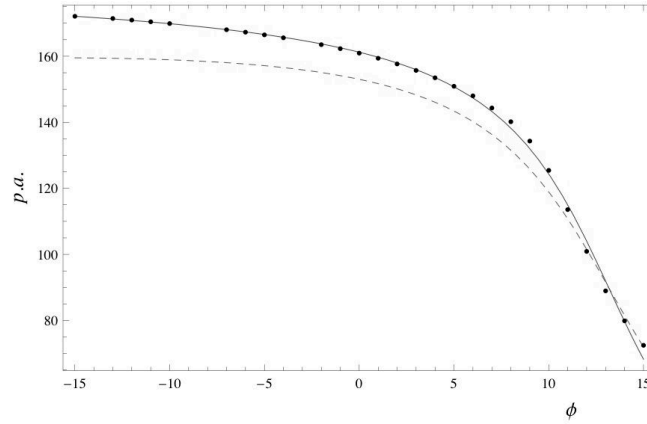


Figure 13. The $p.a.$ curve for $\gamma_0 = 10$, $\lambda = 10^3$, and $\nu = 1\text{GHz}$. Solid line corresponds to the best RVM fit giving unrealistic values $\chi = 93^\circ$ and $\zeta = 97^\circ$. Dashed line corresponds to the RVM curve (1) for real angles $\chi = 45^\circ$ and $\zeta = 48^\circ$

tion the transition from geometrical optics to vacuum propagation, the cyclotron absorption, and the wave refraction simultaneously. Arbitrary non-dipole magnetic field configuration, drift motion of plasma particles, and their realistic energy distribution were taken into account. Using numerical integration, it was shown that the standard S -shape form of the $p.a.$ swing can be realized for small enough multiplicity λ and large enough bulk Lorentz factor γ only. It is also shown that the value of $p.a.$ maximum derivative, that is often used for determination the angle between mag-

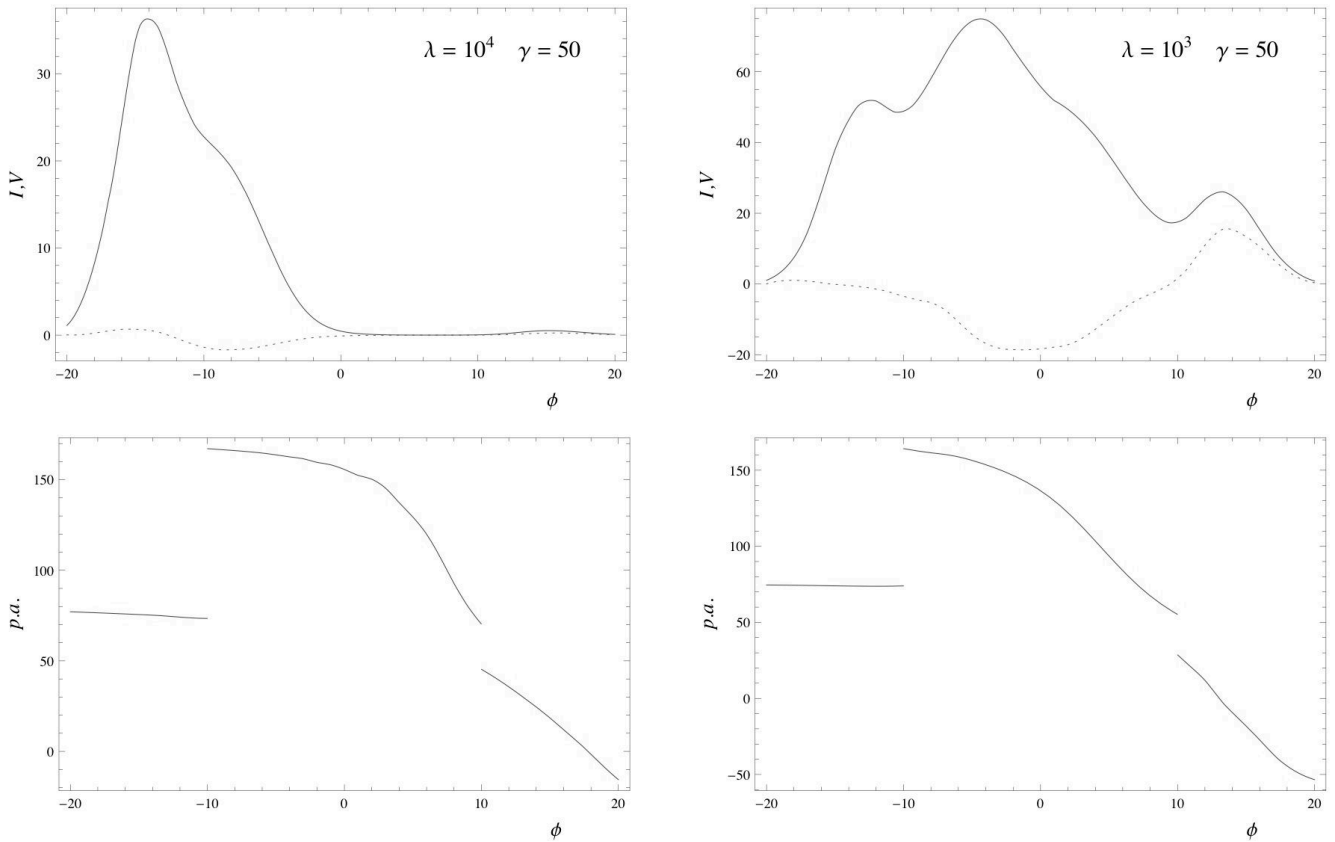
netic dipole and rotation axis, significantly depends on the plasma parameters [and differs from rotation vector model (RVM) value] and, hence, cannot be used without more precise specifying of magnetospheric plasma model.

To summarize, one can formulate the following results:

- We confirm the one-to-one correlation between the signs of circular polarization V and the position angle derivative ($dp.a./d\phi$) along the profile for both ordinary and extraordinary waves. For the X-mode the signs should be the SAME,

Table 4. The position angle maximum derivative $(dp.a./d\phi)_{\max}$ and the shift $\Delta\phi$

λ	γ	ν (GHz)	$(dp.a./d\phi)_{\max}$	RVM	$\Delta\phi$
10^2	50	1	-9.47	-10.14	4.7
10^4	50	1	-14.47	-10.14	7.4
10^5	50	1	-11.70	-10.14	10.5
10^3	10	1	-12.72	-10.14	11.5
10^3	50	1	-9.86	-10.14	4.3
10^3	100	1	-9.47	-10.14	4.7
10^3	300	1	-9.46	-10.14	4.0
10^3	50	0.03	-15.92	-10.14	8.4
10^3	50	0.5	-11.82	-10.14	3.8
10^3	50	0.2	-18.02	-10.14	5.5

**Figure 14.** Main profiles including both modes (O and X ones) for $\lambda = 10^3$ and 10^4 . Here $\gamma = 50$ and $\nu = 1\text{GHz}$

and OPPOSITE for the O-mode. This statement is in good agreement with observations (Han et al., 1998, Andrianov & Beskin, 2010). In some cases, the sign reversal in the core can occur (see Fig. 12 and Wang et al., 2010), that is detected for several pulsars.

- The standard S-shape form of the $p.a.$ swing (1) can be realized for small enough multiplicity λ and large enough bulk Lorentz-factor γ only. In other cases the significant differences can take place. The shift value of the maximum

derivative $(dp.a./d\phi)_{\max}$ can in principle provide us a change of correct enough estimating of plasma parameters.

- In general, the trailing side of the emission beam is absorbed. But in some cases the leading part can be absorbed as well. It happens when the polarization forms close to the light cylinder.

Thus, the approach developed in this article allows the predictions of the theory of radio emission to be quantitatively compared with the observational data. Moreover,

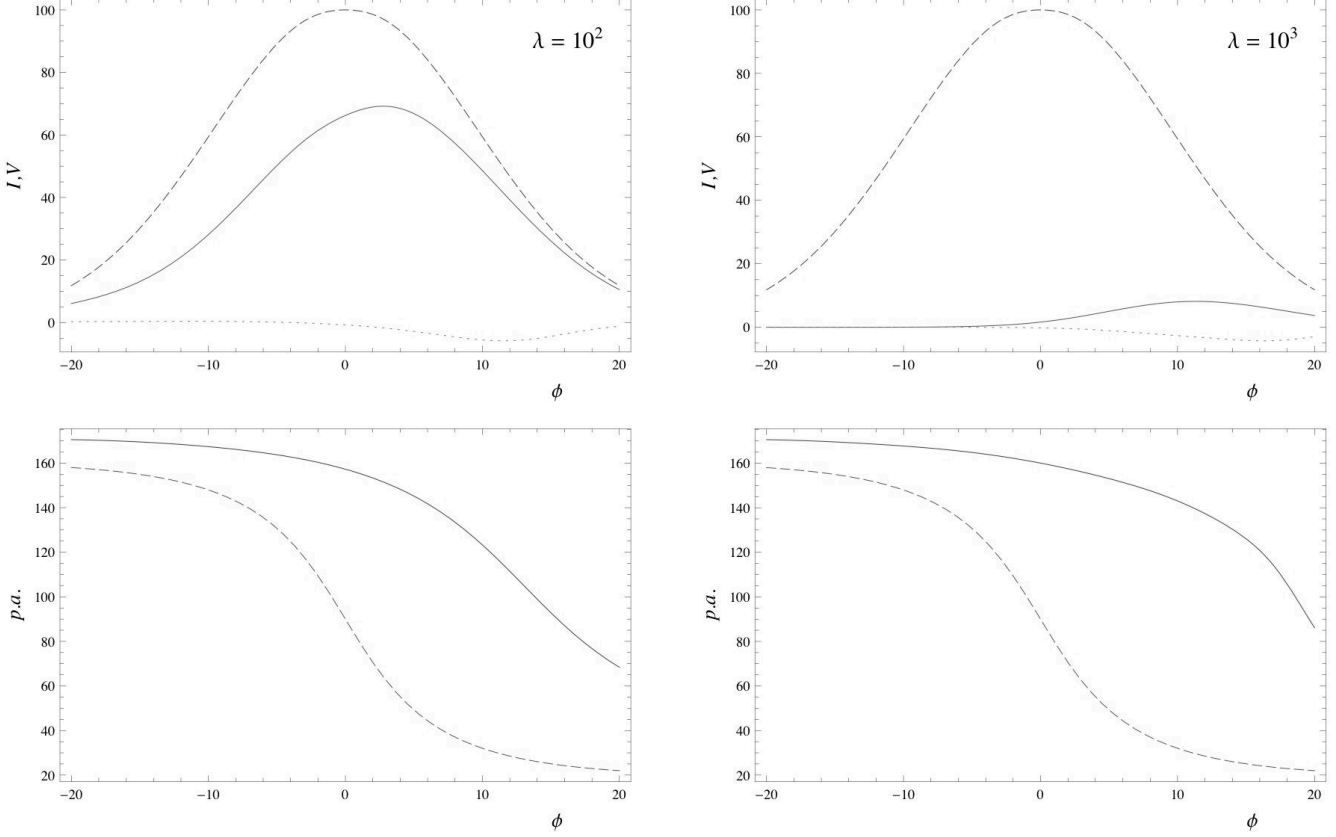


Figure 15. The results of simulations for X-mode for the millisecond pulsar. The multiplicity parameters 10^2 and 10^3

based on the observational data, one can reject a number of models in which the shapes of the profiles of the position angle and the degree of circular polarization never realized in practice are obtained. Thus, it becomes possible to solve the inverse problem, i.e., to determine the parameters of the outflowing plasma and the magnetic field structure. Finally, we will be glad to any collaboration with observers for investigating the observational features of the mean profiles on the base of our theory. The source code of our calculations (in Mathematica 7 or C) is available under request.

7 ACKNOWLEDGMENTS

We thank Prof. A.V. Gurevich and Ya.N. Istomin for his interest and support, and J. Dyks, A. Jessner, V.V. Kocharovskiy, D. Mitra, M.V. Popov, B. Rudak, and H.-G. Wang for useful discussions. We also thanks A. Spitkovsky for valuable opportunity and assistance in dealing with his numerical solution and for outstanding discussions. This work was partially supported by Russian Foundation for Basic Research (Grant no. 11-02-01021).

APPENDIX A: REFRACTION

In this work we consider the simple model of the refraction obtained under the assumption that the plasma number density is constant within the polar cap, i.e., $g(\theta_m, \varphi_m) = 1$. To include refraction into consideration we introduce the

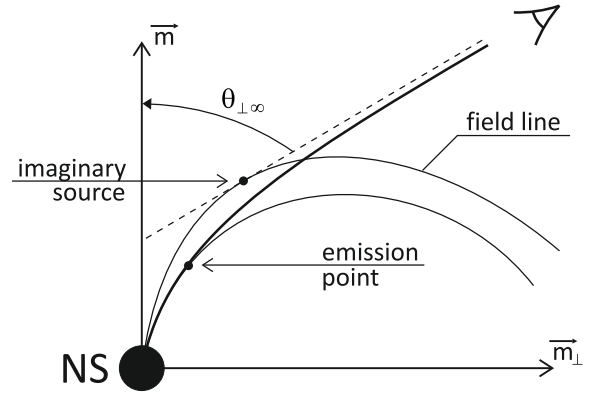


Figure A1. Imaginary source

"imaginary source" of radiation giving the same trajectory at large distances whence emitted parallel to the magnetic field line (see Fig. A1). As the "tearing off" level locates deeply in the magnitosphere, i.e., $r_A \ll R_L$, one can use the analytical expression (22) for the angle $\theta_{\perp\infty}$. It gives for the polar angle of the emission point

$$\theta_{\text{em}} \approx \left[\left(\frac{l_r}{R} \right)^{0.21} \theta_{\perp\infty} \left(\frac{1}{\omega^2} \left\langle \frac{\omega_{p0}^2}{\gamma^3} \right\rangle \right)^{-0.07} \right]^{1.39} \quad (\text{A1})$$

(for dipole magnetic field it does not depend on the radial distance). As a result, we obtain for the polar angle of imaginary source

$$\tan \theta_{\text{im}} = \frac{4}{3} \frac{\tan \theta_{\perp\infty}}{1 + \sqrt{1 + 8/9 \tan^2 \theta_{\perp\infty}}}. \quad (\text{A2})$$

After some algebraic calculations, one can find the trajectory

$$\mathbf{R} = \mathbf{m}(\phi) \rho \cos \theta_{\text{im}} + \mathbf{m}_{\perp}(\phi) \rho \sin \theta_{\text{im}} + r \mathbf{e}_z,$$

where

$$\rho(\phi) = l_t \frac{|\sin \beta - \cos \beta \tan \theta_{\perp\infty}|}{|\tan \theta_{\text{im}} - \tan \theta_{\perp\infty}|} \sqrt{1 + \tan^2 \theta_{\text{im}}} \quad (\text{A3})$$

is the radius of imaginary source, and

$$\beta = \frac{\Psi}{2} + \frac{1}{2} \arcsin \left(\frac{\sin \Psi}{3} \right), \quad (\text{A4})$$

$$\Psi = \theta_{\perp\infty} - \left[\frac{1}{\omega^2} < \frac{\omega_{p0}^2}{\gamma^3} > \left(\frac{l_t}{R} \right)^{-3} \right]^{1/4}. \quad (\text{A5})$$

Finally, $\mathbf{m}_{\perp}(\phi)$ is a unit vector perpendicular to $\mathbf{m}(\phi)$ lying for every pulsar phase ϕ in the plane containing the magnetic $\mathbf{m}(\phi)$ and the wave \mathbf{k} vectors.

APPENDIX B: DERIVATION OF DIELECTRIC TENSOR

Since all the quantities in equation (28) are proportional to $\exp(-i\mathbf{k}\mathbf{r} + i\omega t)$, the solution can be easily obtained:

$$\delta v_x = \frac{1}{\omega_B^2 - \gamma^2 \gamma_U^2 \tilde{\omega}^2} \left[-i\tilde{\omega} \gamma \left(1 + \gamma_U^2 \frac{U_y^2}{c^2} \right) B_1 + \left(\omega_B + i\tilde{\omega} \gamma \gamma_U^2 \frac{U_x U_y}{c^2} \right) B_2 \right], \quad (\text{B1})$$

$$\delta v_y = \frac{1}{\omega_B^2 - \gamma^2 \gamma_U^2 \tilde{\omega}^2} \left[-i\tilde{\omega} \gamma \left(1 + \gamma_U^2 \frac{U_x^2}{c^2} \right) B_2 + \left(-\omega_B + i\tilde{\omega} \gamma \gamma_U^2 \frac{U_x U_y}{c^2} \right) B_1 \right], \quad (\text{B2})$$

$$\delta v_z = i \frac{e \gamma_U^2}{m \omega \tilde{\omega} \gamma^3} [\tilde{\omega} \delta E_z + k_z (\mathbf{V}_0, \delta \mathbf{E})] - \frac{v_{\parallel}}{c^2} \gamma_U^2 (U_x \delta v_x + U_y \delta v_y), \quad (\text{B3})$$

$$B_1 = \frac{e}{m \omega} \left[\tilde{\omega} \delta E_x + k_x (\mathbf{V}_0, \delta \mathbf{E}) - \gamma_U^2 \frac{U_x v_{\parallel}}{c^2} (\tilde{\omega} \delta E_z + k_z (\mathbf{V}_0, \delta \mathbf{E})) \right], \quad (\text{B4})$$

$$B_2 = \frac{e}{m \omega} \left[\tilde{\omega} \delta E_y - \gamma_U^2 \frac{U_y v_{\parallel}}{c^2} [\tilde{\omega} \delta E_z + k_z (\mathbf{V}_0, \delta \mathbf{E})] \right]. \quad (\text{B5})$$

From (31) one can find the number density perturbation

$$\delta n = \frac{n}{\tilde{\omega}} (\mathbf{k}, \delta \mathbf{v}). \quad (\text{B6})$$

After making substitution to (32) we obtain for dielectric tensor components:

$$\varepsilon_{xx} = 1 - \left\langle \frac{\gamma_U^2 k_z^2 U_x^2 \omega_p^2}{\tilde{\omega}^2 \gamma^3 \omega^2} \right\rangle + \left\langle \frac{\omega_p^2 [\tilde{\omega}_0^2 + U_x^2/c^2 (\gamma_U^2 k_z^2 v_{\parallel}^2 - \omega^2)] \gamma \gamma_U^2}{\omega^2 (\omega_B^2 - \gamma^2 \gamma_U^2 \tilde{\omega}^2)} \right\rangle, \quad (\text{B7})$$

$$\varepsilon_{xy} = - \left\langle \frac{\gamma_U^2 k_z^2 U_x U_y \omega_p^2}{\tilde{\omega}^2 \gamma^3 \omega^2} \right\rangle + i \left\langle \frac{\gamma_U^2 \omega_p^2 \omega_B (\tilde{\omega}_0 - \omega U^2/c^2)}{\omega^2 [\omega_B^2 - \gamma^2 \gamma_U^2 \tilde{\omega}^2]} \right\rangle + \left\langle \frac{\omega_p^2 [\tilde{\omega}_0 k_x U_y + U_x U_y/c^2 (\gamma_U^2 k_z^2 v_{\parallel}^2 - \omega^2)] \gamma \gamma_U^2}{\omega^2 (\omega_B^2 - \gamma^2 \gamma_U^2 \tilde{\omega}^2)} \right\rangle, \quad (\text{B8})$$

$$\varepsilon_{xz} = - \left\langle \frac{\gamma_U^2 k_z U_x \omega_p^2 (\omega - k_x U_x)}{\tilde{\omega}^2 \gamma^3 \omega^2} \right\rangle + \left\langle \frac{\omega_p^2 [(\tilde{\omega}_0 - \omega U^2/c^2) v_{\parallel} (k_x - \omega U_x/c^2) + k_z k_x v_{\parallel}^2 U_y^2/c^2] \gamma \gamma_U^4}{\omega^2 (\omega_B^2 - \gamma^2 \gamma_U^2 \tilde{\omega}^2)} \right\rangle - i \left\langle \frac{\gamma_U^2 \omega_B \omega_p^2}{\omega (\omega_B^2 - \gamma^2 \gamma_U^2 \tilde{\omega}^2)} \frac{U_x v_{\parallel}}{c^2} \right\rangle, \quad (\text{B9})$$

$$\varepsilon_{yy} = 1 - \left\langle \frac{k_z^2 \gamma_U^2 U_y^2 \omega_p^2}{\tilde{\omega}^2 \gamma^3 \omega^2} \right\rangle + \left\langle \frac{\omega_p^2 [\tilde{\omega}^2 + U_y^2/c^2 (k_z^2 v_{\parallel}^2 - \omega^2) + k_x^2 U_y^2] \gamma \gamma_U^2}{\omega^2 (\omega_B^2 - \gamma^2 \gamma_U^2 \tilde{\omega}^2)} \right\rangle, \quad (\text{B10})$$

$$\varepsilon_{yz} = - \left\langle \frac{k_z U_y \gamma_U^2 \omega_p^2 (\omega - k_x U_x)}{\tilde{\omega}^2 \gamma^3 \omega^2} \right\rangle + \left\langle \frac{\omega_p^2 [k_x^2 c^2 - \omega^2 + \gamma_U^2 k_z v_{\parallel} (\omega - k_x U_x)] \gamma U_y v_{\parallel} \gamma_U^2}{\omega^2 (\omega_B^2 - \gamma^2 \gamma_U^2 \tilde{\omega}^2) c^2} \right\rangle - i \left\langle \frac{\omega_B \omega_p^2 \gamma_U^2}{\omega^2 (\omega_B^2 - \gamma^2 \gamma_U^2 \tilde{\omega}^2)} v_{\parallel} (k_x - \frac{\omega U_x}{c^2}) \right\rangle, \quad (\text{B11})$$

$$\varepsilon_{zz} = 1 - \left\langle \frac{\omega_p^2 (\omega - k_x U_x)^2 \gamma_U^2}{\omega^2 \tilde{\omega}^2 \gamma^3} \right\rangle + \left\langle \frac{\omega_p^2 [(k_x c - \omega U_x/c)^2 + U_y^2/c^2 (\omega^2 - k_x^2 c^2)] \gamma v_{\parallel}^4 \gamma_U^4}{\omega^2 (\omega_B^2 - \gamma^2 \gamma_U^2 \tilde{\omega}^2) c^2} \right\rangle, \quad (\text{B12})$$

$$\text{Im} \varepsilon_{yy} = -\pi < \frac{\omega_p^2 [\tilde{\omega}^2 + U_y^2/c^2 (k_z^2 v_{\parallel}^2 \gamma_U^2 - \omega^2) + k_x^2 U_y^2] \gamma_U}{\omega^2 \tilde{\omega}} \delta(|\omega_B| - \gamma \gamma_U \tilde{\omega}) >. \quad (\text{B13})$$

$$\text{Im} \varepsilon_{yy} = -\pi < \frac{\omega_p^2 [\tilde{\omega}^2 + U_y^2/c^2 (k_z^2 v_{\parallel}^2 \gamma_U^2 - \omega^2) + k_x^2 U_y^2] \gamma_U}{\omega^2 \tilde{\omega}} \delta(|\omega_B| - \gamma \gamma_U \tilde{\omega}) >. \quad (\text{B14})$$

Here the quantity $\tilde{\omega}_0 = \omega - k_z v_{\parallel}$. Other components of the permittivity tensor are defined by its hermiticity. Therefore, in the expression for gyrofrequency

$$\omega_B = \frac{eB}{m_e c}$$

we should take into the account the sign of the charge e . One

can check that moving to the appropriate reference frame this dielectric tensor reduces to the well-known one (Godfray et al., 1975; Suvorov & Chugunov, 1975; Hardee & Rose, 1975) obtained for the case $\mathbf{E} = 0$.

As a result, one can find for the coefficients in Kravtsov-Orlov equations (73)–(74):

$$\Lambda = -\frac{1}{2} < \frac{\omega_p^2}{\tilde{\omega}^2 \gamma^3} \frac{\gamma_U^2 \omega_B^2}{\omega_B^2 - \gamma^2 \gamma_U^2 \tilde{\omega}^2} > [(\sin \theta - U_x/c)^2 + \cos^2 \theta U_y^2/c^2], \quad (\text{B15})$$

$$\text{Re } \varepsilon_{x'y'} = < \frac{\omega_p^2}{\tilde{\omega}^2 \gamma^3} \frac{\gamma_U^2 \omega_B^2}{\omega_B^2 - \gamma^2 \gamma_U^2 \tilde{\omega}^2} > U_y/c (\sin \theta - U_x/c) \cos \theta, \quad (\text{B16})$$

$$\varepsilon_{y'y'} - \varepsilon_{x'x'} = < \frac{\omega_p^2}{\tilde{\omega}^2 \gamma^3} \frac{\gamma_U^2 \omega_B^2}{\omega_B^2 - \gamma^2 \gamma_U^2 \tilde{\omega}^2} > [(\sin \theta - U_x/c)^2 - \cos^2 \theta U_y^2/c^2], \quad (\text{B17})$$

$$\text{Im } \varepsilon_{x'y'} = < \frac{\omega_p^2}{\omega} \frac{\gamma_U^2 \omega_B}{\omega_B^2 - \gamma^2 \gamma_U^2 \tilde{\omega}^2} > [\cos \theta \gamma_U^{-2} - v_{\parallel}/c (1 - \sin \theta U_x/c)], \quad (\text{B18})$$

$$\tan(2\delta) = -\frac{2U_y/c \cos \theta (\sin \theta - U_x/c)}{(\sin \theta - U_x/c)^2 - \cos^2 \theta U_y^2/c^2}, \quad (\text{B19})$$

$$\tan(\delta) = -\frac{\cos \theta U_y/c}{\sin \theta - U_x/c}. \quad (\text{B20})$$

APPENDIX C: ROTATION OF COORDINATE SYSTEMS

The equations of coordinate transition of the tensor from system in paragraph 3 to the used in 4 are the following

$$\begin{aligned} \varepsilon_{x'x'} &= \varepsilon_{xx} \cos^2 \theta + \varepsilon_{zz} \sin^2 \theta - (\varepsilon_{xz} + \varepsilon_{zx}) \sin \theta \cos \theta, \\ \varepsilon_{y'y'} &= \varepsilon_{yy}, \\ \varepsilon_{z'z'} &= \varepsilon_{xx} \sin^2 \theta + \varepsilon_{zz} \cos^2 \theta + (\varepsilon_{xz} + \varepsilon_{zx}) \sin \theta \cos \theta, \\ \varepsilon_{x'y'} &= \varepsilon_{xy} \cos \theta - \varepsilon_{zy} \sin \theta, \\ \varepsilon_{y'z'} &= \varepsilon_{yx} \sin \theta + \varepsilon_{yz} \cos \theta, \\ \varepsilon_{x'z'} &= (\varepsilon_{xx} - \varepsilon_{zz}) \sin \theta \cos \theta + \varepsilon_{xz} \cos^2 \theta - \varepsilon_{zx} \sin^2 \theta. \end{aligned}$$

Here θ is the angle between ray propagation and local magnetic field directions. Other components of tensor can be defined by its hermiticity.

APPENDIX D: NATURAL MODES

For obtaining natural modes of tensor $\varepsilon_{i'j'}$ it is convenient to rotate the coordinate frame in xy -plane to make the condition $\text{Re } \varepsilon_{x'y'} = 0$ to be valid. One can find that it can be done by rotation defined by the following matrix:

$$M = \begin{pmatrix} \cos a & -\sin a & 0 \\ \sin a & \cos a & 0 \\ 0 & 0 & 1 \end{pmatrix}, \quad (\text{D1})$$

where

$$\tan(2a) = \tan(2\delta) = -\frac{2\text{Re}(\varepsilon_{x'y'})}{\varepsilon_{y'y'} - \varepsilon_{x'x'}}. \quad (\text{D2})$$

In this frame the corresponding expressions for tensor components (defining as $\varepsilon_{i'j'}$) are:

$$\begin{aligned} \varepsilon_{x'x'} &= \varepsilon_{x'x'} \cos^2 a + \varepsilon_{y'y'} \sin^2 a + 2\text{Re}(\varepsilon_{x'y'}) \sin a \cos a, \\ \varepsilon_{y'y'} &= \varepsilon_{x'x'} \sin^2 a + \varepsilon_{y'y'} \cos^2 a - 2\text{Re}(\varepsilon_{x'y'}) \sin a \cos a, \\ \varepsilon_{x'y'} &= i \text{Im}(\varepsilon_{xy}). \end{aligned}$$

The natural modes for this tensor (with poor imaginary $x'y'$ component) are well-known (Andrianov & Beskin (2010), Wang et al. (2010)):

$$\Theta_1 = \beta, \quad \sinh 2\Theta_2 = -\frac{1}{Q}, \quad (\text{D3})$$

$$\Theta_1 = \beta + \pi/2, \quad \sinh 2\Theta_2 = \frac{1}{Q}, \quad (\text{D4})$$

where by the definition

$$Q = i \frac{\varepsilon_{y'y'} - \varepsilon_{x'x'}}{2\varepsilon_{x'y'}}. \quad (\text{D5})$$

It can be easily shown that in our case

$$\frac{1}{Q} = -\frac{\text{Im}[\varepsilon_{x'y'}]}{\Lambda}. \quad (\text{D6})$$

Hence, Eqns. (77)–(78) really define the natural modes in the laboratory frame. The simple expression, which corresponds to a zero plasma temperature for Q is the following (cf. Melrose & Luo 2004 for zero drift):

$$Q = \frac{\lambda \omega_B \omega [(\sin \theta - U_x/c)^2 + U_y^2/c^2 \cos^2 \theta]}{2\gamma^3 \tilde{\omega}^2 [\cos \theta (1 - U^2/c^2) - v_{\parallel}/c (1 - \sin \theta U_x/c)]}. \quad (\text{D7})$$

REFERENCES

- Andrianov A.S., Beskin V.S., 2010, *Astron. Lett.*, 36, 248
- Arons J., Scharlemann E.T., 1979, *Astrophys. J.*, 231, 854
- Asseo E., 1995, *MNRAS*, 276, 74
- Asseo E., Pellat R., Rosado M., 1980, *Astrophys. J.*, 239, 661
- Barnard J.J., 1986, *Astrophys. J.*, 303, 280
- Barnard J.J., Arons J., 1986, *Astrophys. J.*, 302, 138
- Beskin V.S., 1999, *Physics-Uspekhi*, 169, 1169
- Beskin V.S., 2009, *MHD Flows in Compact Astrophysical Objects*, Springer, Berlin
- Beskin V.S., 2010, *Physics-Uspekhi*, 180, 1241
- Beskin V.S., Gurevich A.V., Istomin Y.N., 1988, *Astrophys. and Space Science*, 146, 205
- Beskin V.S., Gurevich A.V., Istomin Y.N., 1993, *Physics of the Pulsar Magnetosphere*, Cambridge University Press
- Beskin V.S., Philippov A.A., 2011, arXiv:1101.5733
- Blandford R.D., 1975, *MNRAS*, 170, 551
- Blaskiewicz M., Cordes J.M., & Wasserman I., 1991, *Astrophys. J.*, 370, 643
- Bogovalov S.V., 1999, *Astron. Astrophys.*, 349, 1017
- Broderick A.E., Blandford R.D., 2010, *ApJ*, 718, 1085
- Budden K.G., 1972, *J. Atm. Terr. Phys.*, 34, 1909
- Cheng A.F., Ruderman M.A., 1979, *Astrophys. J.*, 229, 348
- Contopoulos I., Kazanas D., Fendt Ch., 1999, *Astrophys. J.*, 511, 35
- Czyz Z.H., Bieg B., Kravtsov Yu.A., 2007, *Phys. Lett. A*, 368, 101
- Daugherty J.K., Harding A.K., 1982, *Astrophys. J.*, 252, 337
- Dyks J., Wright G.A.E., Demorest P.B., 2010, *MNRAS*, 405, 509
- Everett J.E., Weisberg J.M., 2001, *ApJ*, 553, 341
- Fussel D., Luo Q., Melrose D.B., 2003, *MNRAS*, 343, 1248
- Ginzburg V.L., 1961, *Propagation of Electromagnetic Waves in Plasma*, Gordon & Breach Science Publishers, New York
- Godfray B.B., Shanahan W.R., Thode L.E., 1975, *Phys. Fluids*, 18, 346
- Goldreich P., Keeley D.A., 1971, *Astrophys. J.*, 170, 463
- Gruzinov A., 2006, *ApJ*, 647, 119
- Gurevich A.V., Istomin Y.N., 1985, *Sov. Phys. JETP*, 62, 1
- Hankins T.H., Rankin J.M., 2010, *AJ*, 139, 168
- Han J., Manchester R., Xu R., Qiao G., 1998, *MNRAS*, 352, 915
- Hardee Ph.D., Rose W.K., 1975, *Astrophys. J.*, 210, 533
- Hibschman J.A., Arons J., 2001, *Astrophys. J.*, 546, 382
- Istomin Y.N., 1988, *Sov. Phys. JETP*, 67, 1380
- Kazbegi A.Z., Machabeli G.Z., Melikidze, G. I., 1991, *MNRAS*, 253, 377
- Keith M. J., Johnston S., Weltevrede P., Kramer M., 2010, *MNRAS*, 402, 745
- Kravtsov Yu.A., Orlov Yu.I., 1990, *Geometrical Optics of Inhomogeneous Media*, Springer, Berlin
- Kuzmin A. D., Dagkesamanskaya I. M., 1983, *Sov. Astron.Lett.* 9, 80
- Landau L.D., Lifshits E.M., 1975, *The Classical Theory of Fields*, Pergamon Press
- Luo Q., Melrose D.B., Machabeli G. Z., 1994, *MNRAS*, 268, 159
- Lyubarskii Yu.E., 1996, *Astron. Astrophys.*, 308, 809
- Lyubarskii Yu.E., 2008, *AIP Conference Proceedings*, 983, 29-37
- Lyne A.G., Graham-Smith F., 1998, *Pulsar Astronomy*, Cambridge University Press
- Malov I.F., 1990, *Sov. Astron.*, 34, 189
- Manchester R., Taylor J., 1977, *Pulsars*, Freeman, San Francisco
- Medin Z., Lai D., 2010, *MNRAS*, 406, 1379
- Melrose D.B., Luo Q., 2004, *MNRAS*, 352, 915
- Michel F.C., 1973, *Astrophys. J.*, 180, L133
- Mikhailovsky A.B., Onishchenko O.G., Suramlioshvili G.I., Sharapov S.E., 1982, *Sov. Astron. Lett.*, 8, 685
- Petrova S.A., 2001, *Astron. Astrophys.* 378, 883
- Petrova S.A., 2003, *Astron. Astrophys.* 408, 1057
- Petrova S.A., 2006, *MNRAS* 368, 1764
- Petrova S.A., Lyubarskii Yu.E., 1998, *Astron. Astrophys.*, 333, 181
- Petrova S.A., Lyubarskii Yu.E., 2000, *Astron. Astrophys.*, 355, 1168
- Ruderman M.A., Sutherland P.G., 1975, *Astrophys. J.*, 196, 51
- Sazonov V.N., 1969, *Sov. Phys. JETP*, 29, 578
- Shcherbakov R.V., Huang L., 2011, *MNRAS*, 410, 1052
- Spitkovsky A., 2006, *Astrophys. J.*, 648, L51
- Sturrock P.A., 1971, *Astrophys. J.*, 164, 529
- Suvorov E.V., Chugunov Yu.M., 1975, *Astrophysics*, 11, 203
- Taylor J.H., Stinebring D.R., 1986, *Ann. Rev. Astron. Astrophys.*, 24, 285
- Timokhin A.N., 2006, *MNRAS*, 368, 1055
- Usov V.V., 2006, *Proceedings of the 26th meeting of the IAU, Prague, Czech Republic*
- Wang Z., Lai D., Han J., 2010, *MNRAS*, 403, 2
- Wang Z., Lai D., Han J., 2011, *MNRAS*, (in press)
- Weltevrede P., Johnston S., 2008, *MNRAS*, 391, 1210
- Yan W. M., Manchester R.N., van Straten W. et al., 2011, *MNRAS* 467 (in press)
- Zheleznyakov V.V., 1970, *Radio Emission of the Sun and Planets*, Pergamon, Oxford
- Zheleznyakov V.V., 1996, *Radiation in Astrophysical Plasmas*, Springer, Berlin
- Zheleznyakov V.V., Kocharovsky V.V., Kocharovsky V.I., 1983, *Sov. Phys. Uspekhi*, 141, 257